CERN 73-14
Laboratory I
Track Chambers Division
7 November 1973

ORGANISATION EUROPÉENNE POUR LA RECHERCHE NUCLÉAIRE
CERN EUROPEAN ORGANIZATION FOR NUCLEAR RESEARCH

A STUDY OF SYSTEMATIC AND RANDOM ERRORS OF THE CERN 2 METRE HYDROGEN BUBBLE CHAMBER

G. Ekspong, L. Voyvodic and J. Zoll

GENEVA

1973

CERN 73-14
Laboratory I
Track Chambers Division
7 November 1973

ORGANISATION EUROPÉENNE POUR LA RECHERCHE NUCLÉAIRE

CERN EUROPEAN ORGANIZATION FOR NUCLEAR RESEARCH

A STUDY OF SYSTEMATIC AND RANDOM ERRORS OF THE CERN 2 METRE HYDROGEN BUBBLE CHAMBER

G. Ekspong*), L. Voyvodic**) and J. Zoll

GENEVA

1973

---

*) On leave from Institute of Physics, University of Stockholm, Sweden.

**) On leave from Argonne National Laboratory, Illinois, USA.

CERN - Service d'Information scientifique H/550 - 2300 - novembre 1973

CONTENTS

INTRODUCTION

Two circumstances call for a better understanding of errors in bubble chamber experiments. One is the trend towards higher energies where systematic errors are relatively more important than at lower energies. The second is that, even at medium energies, systematic errors may show up when one is dealing with large samples.

Previous experience has demonstrated the existence of systematic errors in the measured physical quantities; however, most of this work is not published. Observations have related to systematic errors in a variety of quantities such as beam momentum, secondary particle momenta, and dip angles along tracks, and in losses of the number of kinematically highly constrained events[1-3].

Two series of exposures were made with the CERN 2 m bubble chamber in order to search for causes of disturbances depending on the operating conditions and to find, if possible, optimized running conditions. In the first series the chamber was filled with deuterium, in the second with hydrogen. Chapter I is devoted to the deuterium results and contains a description of the methods used for precise error analysis. Chapter II contains the results from the hydrogen tests.

CHAPTER I

TESTS IN A DEUTERIUM-FILLED CHAMBER

G. Ekspong, L. Voyvodic and J. Zoll

1. THE EXPOSURES

The beam consisted of 16 GeV/c pions obtained from the RF-separated beam line (u_5). The choice of high energy was dictated by the wish to keep multiple scattering effects relatively small. The chamber was run in the double expansion mode, i.e. two expansions for each PS pulse. No magnetic field was applied to the chamber, so that spurious curvatures could show up in a reasonably unambiguous way. The chamber cameras were the ones that were newly installed in 1969. The big chamber windows carrying the fiducial marks were the second set, also installed in 1969.

A series of 10 runs, each with about 500 pictures, were made with different timings as shown in Fig. 1. Three delay times between beam arrival and flash triggering were used, namely 0.8 msec, 1.5 msec, and 2.0 msec. About 1.2 msec is normal for this chamber. Three such runs were made under symmetric conditions, i.e. with beam and flash on either side of the time for pressure minimum in the expansion cycle. A fourth run under symmetric conditions with a 1.5 msec flash delay was made at the very end of the test series. Another three runs were made with both the beam and flash early in the expansion cycle. In this case the beam arrival was fixed to occur 2 msec before pressure minimum and with the three flash delays applied in turn. Finally, three runs were made with beam and flash late in the expansion cycle. The flash triggering was fixed to occur 2 msec after pressure minimum, and beam arrivals were adjusted to occur 0.8 msec, 1.5 msec, and 2.0 msec before the flash. In referring to the different rolls, two code letters are used. The first letter indicates the position with respect to the expansion curve (E, S, L denote early, symmetric, and late, respectively); the second letter identifies the flash time delay (S, M, L denote short, medium, and long, respectively).

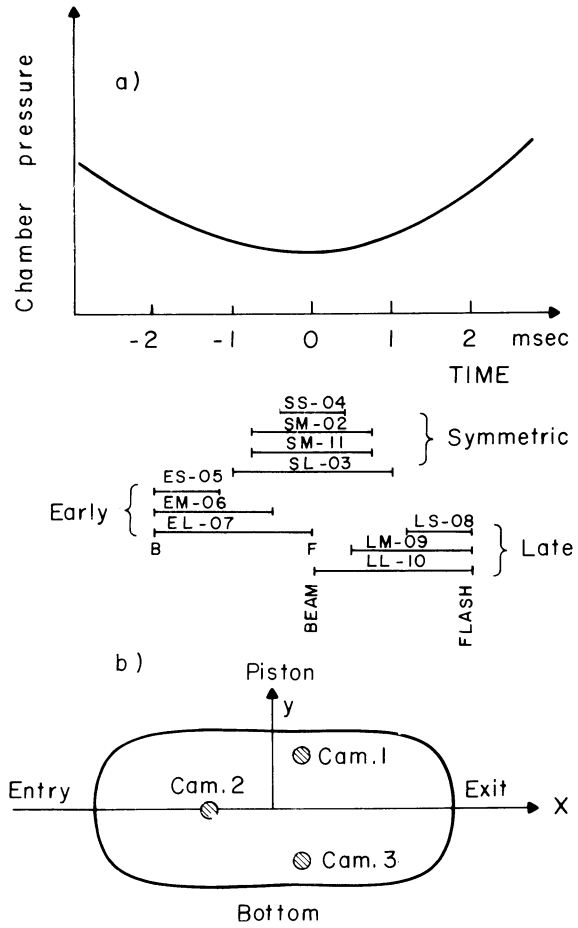

Fig. 1

a) Timing conditions relative to the chamber pressure curve for the 10 runs. Code names are given by the letters. The first letter defines the set (early, symmetric, late), the second letter defines the flash time delay (short, medium, long).

b) Coordinate system used with the y-axis pointing up towards the piston. Approximate camera positions indicated.

2. THE MEASUREMENTS

In each roll (10 in all) of about 500 pictures, up to about 800 tracks were selected and predigitized on the CERN "Milady" scanning tables. Only non-interacting beam tracks with no visible scattering were selected. The tracks were spread in the transverse y-coordinate over some 20 cm in chamber space, and their measured length was about 163 cm.

The tracks were measured on each view by the CERN measuring machines HPD 1 and HPD 2. The rolls with the shortest flash delays of 0.8 msec had rather faint tracks, which led to the failure of roll ES-05 on HPD 2. With the exception of roll ES-05, all rolls were thus measured twice. Using this precaution, one can separate with greater confidence the systematic errors caused by liquid motion, from those due to the measuring machines.

From the HPD digitizings, about 50 master points per view and track were computed, using the program SMOG. These were then used for the space reconstruction of tracks. A modified version of the program THRESH was used to construct a straight line fit in space.

The preset radius of curvature in THRESH used to represent straight lines was 10^9 cm, corresponding to a negligible sagitta in the film plane. Together with the tracks, 10 fiducial marks per view were measured. These were used for the transformation from film to the

chamber reference plane (the THRESH six-parameter linear transformation). The optical parameters and distortion parameters needed for the space reconstruction were obtained by extensive measurements of fiducial marks prior to the track measurements, as described in the next section.

3. OPTICAL AND DISTORTION PARAMETERS

All visible fiducial marks in all three planes (two planes on the front window, one on the back window) were measured in about 50 frames in each roll. The title for optical reconstruction was then produced, separately for each of the two HPD's, using the program PYTHON. Exactly the same optical constants were used for all rolls when measured on the same HPD. The values of the optical constants are given in Table 1. The distortion parameters are collected in Table 2.

As a partial check on the accuracy and also on the assumption that the same set of distortion parameters can be used for all rolls, the following tests were made. The measured positions of all fiducials in all frames were superimposed on each other using six-parameter linear transformations in x and y. The number of fiducial marks measured were 6 in plane 1, 15 in plane 2, and 9 in plane 3. The resulting standard deviations in the positions on the film plane are given in Table 3. The best results hold in view 3, where the standard deviations in either the x- or the y-direction are in the range 0.8 to 1.2 μm on plane 2 fiducials. The corresponding results for the other views are in the range 1.3 μm to 1.9 μm. Backwindow fiducials show larger deviations in the range 1.9 to 2.8 μm. These crosses may be expected to scatter more in image positions as they are viewed through 60 cm of liquid. As illustrated by the results from roll EM-06, the standard deviations in a single roll are

Table 1

Optical constants used in track reconstruction

HPD	Camera	Camera positions (cm)			Media properties	
		x	y	z	Index	Thickness (cm)
1	1	13.1668	28.9996	243.5358	1.0000	219.0120
	2	-31.8482	0.0055	243.5283	1.5259	∿ 7.5000 a)
	3	13.1701	-29.0018	243.5510	1.5324	17.0278
					1.1110	50.7400 b)
2	1	13.1680	29.0002	242.5741	1.0000	218.0503
	2	-31.8460	0.0039	242.6113	1.5259	∿ 7.5000 a)
	3	13.1673	-28.9977	242.6168	1.5324	17.0278
					1.1110	50.5400 b)

a) More precisely for the three views: 7.4960, 7.5509, 7.5562

b) By accident, a slightly different chamber depth has been used when making the titles for HPD 1 and HPD 2. This reflects into different distances lens to chamber. This is annoying, but of no consequence for the present study.

Table 2

Distortion parameters used in track reconstruction

HPD	Camera	x tilt parameter α_1	y tilt parameter α_2	Lens distortion parameter α_3	Parabolic parameter α_4
1	1	-0.00038	-0.00052	-0.00776	0.00012
	2	+0.00046	+0.00182	-0.00740	-0.00081
	3	-0.00021	+0.00152	-0.00557	-0.00038
2	1	-0.00044	-0.00238	-0.00728	0.00106
	2	+0.00030	-0.00006	-0.00698	0.00005
	3	-0.00019	-0.00027	-0.00472	0.00038

The coefficients α_i are used in the following formula:

$$\begin{pmatrix} x' \\ y' \end{pmatrix} = \left[1 + \alpha_1 x + \alpha_2 y + \alpha_3 (x^2 + y^2)\right] \begin{pmatrix} x \\ y \end{pmatrix} + \begin{pmatrix} 0 \\ \alpha_4 x^2 \end{pmatrix} ,$$

with

$$(x/y) = \frac{1}{f} (X/Y), \qquad (x'/y') = \frac{1}{f} (X'/Y');$$

where f is the film-to-lens distance and (X/Y) are the measured film coordinates, transformed to the standard film system by a six-parameter linear transformation. For each film this system is centred on the optical axis of the lens, the direction of the x-axis is defined by the standard coordinate system in space. (X'/Y') are the corrected film coordinates.

Table 3

Measurement accuracy of fiducial marks given as standard deviations on film (in μm). About 50 frames per roll of film were measured. The number of fiducial marks measured are 15 in plane 2 and 9 in plane 3.

	View 1		View 2		View 3	
	σ_x	σ_y	σ_x	σ_y	σ_x	σ_y
Plane 2 (front window)						
HPD 1 (5 rolls)	1.5	1.5	1.6	1.9	1.0	1.2
HPD 2 (10 rolls)	1.3	1.3	1.3	1.6	0.8	0.9
HPD 1 (roll EM-06)	1.4	1.5	1.4	1.7	0.9	1.0
HPD 2 (roll EM-06)	1.2	1.1	1.2	1.3	0.8	0.8
Manual setting on LSD (roll EM-06)	4.0	4.2	4.5	4.6	3.9	4.0
Plane 3 (back window)						
HPD 1 (5 rolls)	2.4	2.3	2.4	2.4	2.1	2.1
HPD 2 (10 rolls)	2.8	2.2	2.3	2.1	1.9	1.9
HPD 1 (roll EM-06)	2.5	2.5	2.5	2.5	2.1	2.0
HPD 2 (roll EM-06, UP)	3.5	3.3	3.5	3.0	2.2	2.3
HPD 2 (roll EM-06, MID)	2.2	2.0	2.0	2.0	1.7	1.6
HPD 2 (roll EM-06, LOW)	1.8	1.9	1.8	1.5	1.8	1.6
Manual setting on LSD (roll EM-06)	5.8	6.2	6.0	6.8	5.8	6.1

only slightly smaller than those for the set of all rolls (and are sometimes larger, as in the case of plane 3 measured on HPD 1). The HPD accuracy is seen to be very high. For the purpose of comparison, results from manual settings on the CERN spiral reader are also given in Table 3.

Several distortion parametrizations were tried containing from three to nine parameters per view. Using the PYTHON-produced optical constants, the fiducial marks on plane 2 and plane 3 were reconstructed in space and compared with their known positions. The differences in the x-, y-, and z-coordinates then measure the precision, to the extent that the known positions can be regarded as error-free (errors in the known x- and y-positions are of the order of 50 μm). The standard deviations obtained as an average over all fiducial marks in a given plane are collected in Table 4. Increasing the number of distortion parameters improves the precision, but only to the extent expected from the loss of degrees of freedom, and even only up to seven parameters. In order not to over-parametrize, the final studies of track profiles were made with the four-parameter formula:

$$\begin{pmatrix} x' \\ y' \end{pmatrix} = \left[1 + \alpha_1 x + \alpha_2 y + \alpha_3 (x^2 + y^2)\right] \begin{pmatrix} x \\ y \end{pmatrix} + \begin{pmatrix} 0 \\ \alpha_4 x^2 \end{pmatrix} .$$

(All the coordinates are normalized to a common distance, making the coefficients α_i dimensionless.)

The values of the four parameters α_i are given in Table 2. It is noted that the parabolic correction term $\alpha_4 x^2$ is important for our study of spurious curvatures. It is view-dependent and also strongly dependent on which of the two HPD's is used. We consider it necessary to make this correction so that spurious curvatures occurring in the measuring

Table 4

Precision of reconstructed fiducial marks given as standard deviations in space (μm) for different distortion formulae with n parameters (n = 4 is used in the final studies)

	Plane 2			Plane 3		
	x	y	z	x	y	z
HPD 1						
n = 3	16	45	145	17	61	215
n = 4	12	31	112	25	46	182
n = 7	8	10	62	20	19	105
n = 9	8	10	67	19	18	100
HPD 2						
n = 3	25	38	135	30	35	200
n = 4	20	18	107	31	28	167
n = 7	8	10	67	20	19	110
n = 9	11	12	66	23	22	105

machines or cameras get eliminated. As an example showing the magnitude of the curvatures expressed by α_4, a value $\alpha_4 = 0.001$ would correspond to a curvature $\rho^{-1} = 8 \times 10^{-6}$ cm^{-1} ($\rho = 1200$ m); or in other words, to a sagitta on full-length tracks of about 20 μm on the film. The value of α_4 is strongly view-dependent. Thus only after making this correction can one hope to get reasonably view-independent results for any remaining track distortion. It is noted that the parabolic correction in the α_4 term is also dependent on which measuring machine is used. While these studies were in progress, it was found that HPD 2 distorted straight lines into curved shapes and also that the fiducial pattern became distorted[4]. This, however, occurs with remarkable reproducibility, frame after frame. Our comparison of HPD 1 and HPD 2 uncorrected fiducial patterns confirms the behaviour found in Ref. 4.

4. TREATMENT OF HPD MEASUREMENTS AND FIRST RESULTS

About 50 master points per view were used in the space reconstruction of a straight line to represent the track. The quantities of greatest interest for the study of systematic and random errors are the individual residuals, about 150 for each track. These are recorded on the THRESH output tape (in μm on the film plane) together with the corresponding track lengths. The definition is residual r = [y(measured) - y(fitted)] with the y-axis pointing in the direction from the chamber centre up towards the piston. Other quantities recorded on the tape are the track parameters: the starting coordinates, the azimuth angle, and the dip angle. The average residual on each track was also computed and recorded. This quantity is defined as the square root of the average sum of squared residuals for all points in all three views. If no significant systematic errors were present, the track-averaged residual, further averaged over a given sample, should be close to that expected from random errors. This does not hold true, thus indicating the presence of systematic errors. It is, however, no great surprise that such errors exist. The problem is to establish which of several possible sources of systematic errors is important, and furthermore to find out if such an error is a constant error, or in other words, to what degree a random error component is associated with it.

This program leads to a general study of systematic and random errors and their possible sources. One difficulty is to disentangle several possible sources which may cause systematic distortion of the tracks, and to do this in the presence of random errors. The latter are identified and eliminated by the study of a large enough sample of tracks under identical conditions. An observed spurious curvature in such a sample could be due to bulk motion of the chamber liquid, to thermal turbulence, to non-linear film distortions, to uncorrected optical distortions, or to other reconstruction inaccuracies. If the liquid properties are important, one expects the systematic effects to show up in a similar way in all three views. If bulk liquid motion plays a role, one expects the systematic error to change in size with increasing flash delay. Obviously, the present set of exposures is suitable for making a search to identify the source (or sources) of errors and possibly to find conditions when the errors are smallest. Before final treatment each sample was re-defined so that tracks deviating too much from Gaussian distributions (due, for example, to single scatterings) were eliminated. This cleaning procedure is of vital importance for the analysis of random errors, as it rejects about 2% of tracks which sit in the non-Gaussian tail. The method is described in Section 5.3.

5. ANALYSIS OF RESIDUALS

The residuals contain information on both random and systematic errors. In any individual track the two types of error are mixed in an inseparable manner. It is necessary to treat a sample of tracks in order to disentangle one type from the other.

5.1 The mean track profile

In order to study the systematic behaviour of the tracks, use was made of a graphic representation of the "mean track profile", showing the systematic deformations of all the tracks of a given sample as a function of x, the chamber coordinate in the beam direction.

The chamber was divided into 36 x-slices of 5 cm width each, from x = -90 cm to x = +90 cm. Within each slice, the mean and the r.m.s. scatter of the residuals of all the tracks of a given sample were computed; this was done separately for each camera. The resulting mean residual as a function of x, $\bar{r}(x)$, is called the mean track profile. This is fairly free from random errors, as the effects of multiple scattering and of the measurement error are averaged out.

The first samples treated were the 10 above-mentioned rolls, summarized in Fig. 1. In order to study variations of the track behaviour depending on the distance of the tracks from the piston, each roll was subdivided into three about equally large samples (UP, MID, LOW) containing the tracks in the upper, middle, and lower part of the chamber; more precisely, the y-intervals ⟨25, -2, -9, -25⟩. Thus for each roll we have four mean track profiles to look at; for example, the early roll with long flash delay gives the four samples EL-ALL, EL-UP, EL-MID, EL-LOW. A look at the track profiles gives a number of first qualitative results:

- Deviations of the profiles from the ideal straight line are clearly significant by many standard deviations. The mean residuals go up to 10 μm on the film; their standard deviation is about 0.2 μm.
- A systematic translation of all residuals -- about +2 μm in views 1 and 3, -4 μm in view 2 -- is present uniformly throughout all rolls, pointing to a small and harmless optical defect. This has been eliminated in all further treatments.
- Most rolls show a clear curvature. This curvature changes from one roll to the next, and also within one roll between the three sub-samples UP, MID, LOW. These changes of curvature point to condition-dependent global deformations of the tracks, and these have been analysed in detail. Figure 2 shows examples of profiles.
- The degree to which the various views agree on the detailed shapes of the track profiles is shown in Fig. 3. Here the profile differences between views for a given track sample are plotted as a function of the chamber coordinate x. All data points lie between the error bars in the figure. Some view-dependent optical defects seem to exist with a magnitude of about 2 μm.
- The profiles show minor bumps and departures from the global parabolic shapes. These often occur in the region right under the piston and could be due to local jets of liquid. The magnitude is usually less than 3 μm on the film, which corresponds to 40 μm in chamber space.

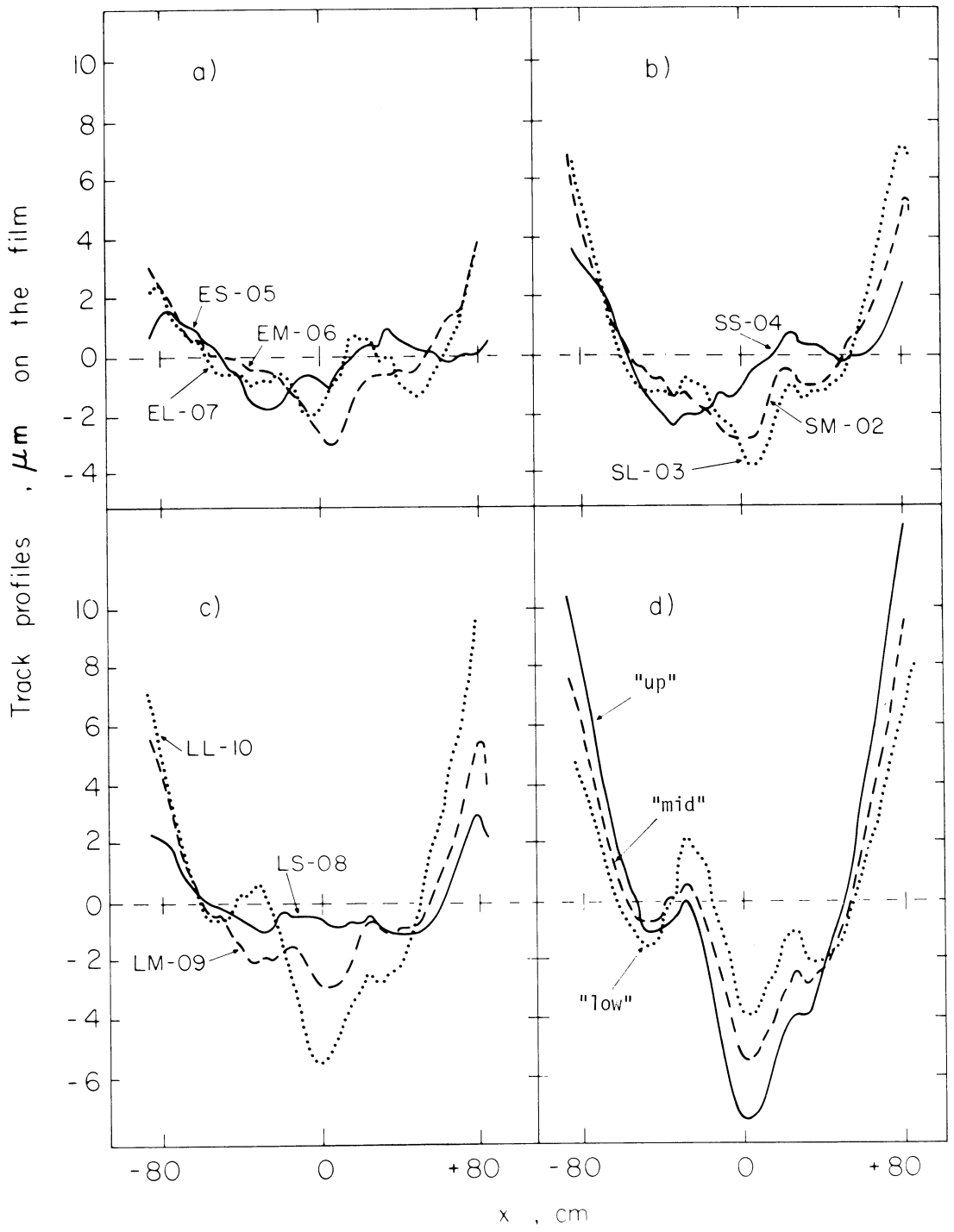

Fig. 2 Track profiles showing the mean residual of a large sample of tracks as a function of x. The profiles are shown as hand-drawn lines through the points obtained for 5 cm intervals; each such point has a statistical error of ±0.2 μm:

a) early exposures, middle of chamber, measurements on view 1 with HPD 1;

b) symmetric exposures, middle of chamber, measurements on view 1 with HPD 2;

c) late exposures, middle of chamber, measurements on view 1 with HPD 2;

d) profiles for tracks at top (near the piston) ("up"), in the middle ("mid"), and at bottom ("low") of the chamber -- late exposures with long flash delay -- measurements done on view 1 with HPD 2.

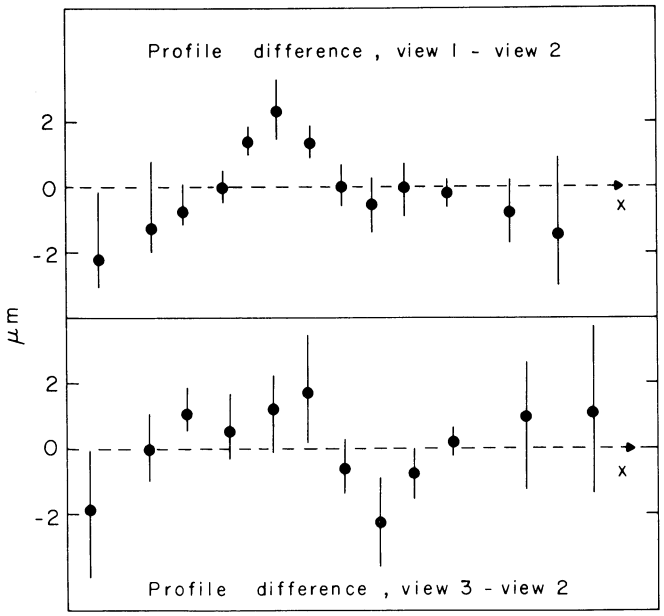

Fig. 3

Track profile differences between views for a given sample. Points are placed at the modes and error bars at the full range of nine differences (HPD 2 data):
a) the view 1 - view 2 differences
b) the view 3 - view 2 differences

5.2 Measurement of curvature

For all tracks in the sample, a parabola $r = a + bx + cx^2$ has been fitted to the residuals for each view; the parameter c measures the curvature of the residuals on the film. Both systematic and random effects are at work to make $c \neq 0$ on any individual track. Multiple scattering and liquid motion effects should make the c's of the three views highly correlated. On the other hand, the mean value of c in a sample is a measure of systematic effects. The experimentally found distributions of c turned out to be Gaussian-like with a few tracks in long tails. This observation is consistent with the presence of a few tracks with small-angle scattering. These were removed from the sample.

We already know c to be some function of the y-position of the track, which indicates a deformation of the track depending on its distance from the piston. To be sure of the shape of this function, the mean values of c over 2 cm intervals of y have been plotted for two rolls. The result is that a linear representation of this function is adequate on all three views. Therefore, we fit a regression line of the form $c = c_0 + c'y_c$ using all good tracks of a roll, with y_c the y-coordinate of the track at the middle of the chamber. In this way the two parameters c_0 and c' were obtained for each roll and each view, representing the mean systematic curvature at the centre of the chamber ($y = 0$) and the gradient of curvatures.

5.3 Purification of the samples

Two criteria were used simultaneously. A track is rejected:

a) if any of the three curvatures c deviate from the expected values $c_0 + c'y_c$ by more than a given tolerance t, about 3 standard deviations;

b) if the r.m.s. "new residual" is bigger than 6 μm. The "new residual" is obtained by subtracting out the parabolic fit to the track: $r'(x) = r(x) - a - bx - cx^2$. The

average r.m.s. new residual is about 2 μm. This second criterion acts as a (presumably unnecessary) safety precaution.

These criteria reject tracks with small-angle or one-sided plural scattering, and badly measured tracks. In finer detail, there is feedback between the criterion for purification and the desired quantities c_0 and c'. In order to find the correct parameters c_0 and c' for all three views, and the elements of the three-dimensional covariance matrix of the curvature distribution, a systematic search has been made by plotting all desired quantities as functions of the tolerance parameter t for criterion (a). This parameter t was varied in small steps from roughly 10 standard deviations to somewhat less than 1 standard deviation. The corresponding theoretical functions -- var (c), cov (c_i, c_j), and cor (c_i, c_j) -- for truncated binormal distributions were computed. Comparison allowed the true asymptotic values of the variances and covariances to be determined. This gives the values of the tolerance parameters t, and hence the desired values c_0 and c'.

5.4 Data for further analysis

The procedures described in Section 5 yield the data from which the conclusions will be drawn. This discussion of results is conveniently divided into the discussion of systematic effects (Section 6), and random effects (Section 7).

Data on the systematic deformations of the tracks are the c_0 and c' giving the global deformations, and the "corrected mean track profiles" (parabolic effects subtracted out) showing the local systematic deformations.

Data on the random effects are the variances and the inter-view covariances of the c, and also the variances of the "straight line residuals". These residuals are obtained by fitting a straight line $a_s + b_s x$ to the residuals of each track of the purified sample, and subtracting out the straight line effects in order to get $r_s(x) = r(x) - a_s - b_s x$ *).

6. SYSTEMATIC ERRORS (SPURIOUS CURVATURES)

The curvature parameter c_0 represents the curvature ρ_0^{-1} through the relation $\rho_0^{-1} = 2 \cdot M \cdot c_0$, where M is the magnification from film plane to chamber space. Its magnitude is M = 13.1. Values of c_0 and c' are obtained for each roll and each view. The corresponding curvatures ρ_0^{-1} and curvature gradients $d\rho^{-1}/dy$ are given in Table 5. These values were obtained by parabolic fits in each view to the full length of the tracks, about 163 cm in space. The table values represent the mean values of a sample of 400 to 800 tracks. The values of $1/\rho_0$ are found to be in the range from about -1×10^{-6} cm^{-1} to $+9 \times 10^{-6}$ cm^{-1}. Alternatively, one could have represented the results as the sagittas, the relation being $s_0 = \rho_0^{-1} \times L^2/8 = 1/\rho_0 \times 3.32 \times 10^3$ cm. The sagittas are thus found to be in the range from -30 μm to +300 μm (in space). The experimental values given in Table 5 show a fair amount of internal consistency. The trends are roughly the same in all three views and similar for both measuring machines (HPD 1 and HPD 2). The inter-view comparisons, roll by roll, are shown in Fig. 4

*) The constants a_s are identical with the view-dependent translations mentioned in Section 6.1. The rotation parameters b_s were found to be small: $< 10^{-5}$ rad.

Table 5

Systematic errors.
Spurious curvatures of no-field tracks in the CERN 2 m DBC.
ρ_0^{-1} = curvature at the centre (y = 0) in units of 10^{-6} cm^{-1}
$d\rho^{-1}/dy$ = curvature gradient in units of 10^{-7} cm^{-2}

		Average curvature, ρ_0^{-1}				Curvature gradient			
Roll	HPD	View 1	View 2	View 3	All-view aver.	View 1	View 2	View 3	All-view aver.
ES-05	1	0.8	1.3	1.6	1.2	0.2	-0.8	-0.4	-0.3
EM-06	1	1.7	1.3	2.4	1.8	0.1	-1.0	-0.6	-0.5
EL-07	1	1.8	0.8	3.0	1.9	0.8	-0.4	0.4	0.2
SS-04	1	4.2	4.5	5.5	4.7	1.3	0.4	0.7	0.8
SM-02	1	4.8	5.4	5.9	5.4	1.9	0.8	1.5	1.4
SM-11	1	4.9	6.2	7.8	6.3	2.0	1.2	1.8	1.7
SL-03	1	5.1	5.2	6.7	5.7	1.8	0.8	1.8	1.5
LS-08	1	4.1	5.1	5.4	4.8	1.9	0.6	1.1	1.2
LM-09	1	6.0	7.9	8.5	7.3	3.0	1.9	2.2	2.4
LL-10	1	8.0	9.4	9.6	9.0	3.1	1.8	2.1	2.3
EM-06	2	2.9	1.7	1.3	2.0	0.4	-0.7	0.0	-0.1
EL-07	2	-0.8	-1.3	0.4	-0.6	0.6	-0.4	0.5	0.2
SS-04	2	2.1	2.8	3.0	2.6	1.1	0.5	0.7	0.8
SM-02	2	3.6	5.0	3.8	4.1	1.8	0.7	1.6	1.4
SM-11	2	3.2	3.6	5.7	4.2	2.2	1.1	1.8	1.7
SL-03	2	4.2	4.5	5.0	4.6	1.9	0.8	1.9	1.5
LS-08	2	2.0	3.2	3.3	2.9	2.0	0.6	1.0	1.2
LM-09	2	4.5	5.7	6.7	5.6	3.3	1.9	2.4	2.5
LL-10	2	5.8	6.6	7.7	6.7	3.0	1.9	2.2	2.4

for the curvatures. The inter-view correlations are summarized by giving the regression lines the following linear form:

$$\rho_0^{-1}(\alpha) = K_\alpha \, \rho_0^{-1}(3) + L_\alpha \qquad \text{(view number } \alpha = 1,2) \quad .$$

Least squares fits obtained with equal weight to all points (except roll EM-06 in HPD 2, which is given zero weight) result in the following values for the slopes K_α and intercepts L_α:

For HPD 1: $K_1 = 0.80$ $L_1 = -0.4 \times 10^{-6}$ cm^{-1}

$K_2 = 1.04$ $L_2 = -1.2 \times 10^{-6}$ cm^{-1}

For HPD 2: $K_1 = 0.81$ $L_1 = -0.5 \times 10^{-6}$ cm^{-1}

$K_2 = 0.94$ $L_2 = -0.4 \times 10^{-6}$ cm^{-1} .

The deviations of points from the regression lines in Fig. 4 indicate a standard deviation in each ρ_0^{-1} of 0.4×10^{-6} cm^{-1} (HPD 1) and 0.7×10^{-6} cm^{-1} (HPD 2), respectively. These errors are much larger than the purely statistical errors derived from the curvature distributions in each individual roll which, with the given sample sizes, yield a standard error in the mean of only 0.1×10^{-6} cm^{-1}.

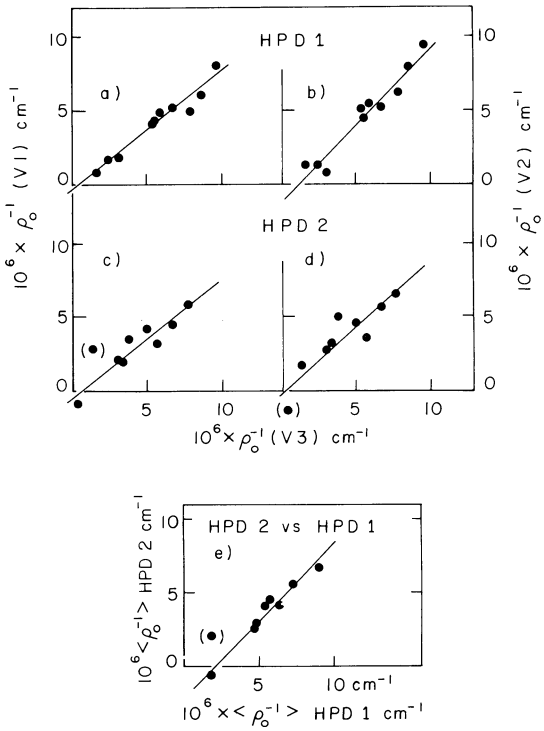

Fig. 4

Spurious curvatures in various views and rolls, measured on two HPD's. Inter-view regressions shown for

a) view 1 versus view 3 on HPD 1,
b) view 2 versus view 3 on HPD 1,
c) view 1 versus view 3 on HPD 2,
d) view 2 versus view 3 on HPD 2,

and comparison of the two measuring machines in (e) using view-averaged curvatures.

The curvature gradients in Table 5 show similar correlations between views. The regression lines in Fig. 5 have slopes K_α and intercepts L_α as follows:

For HPD 1: $K_1 = 0.98$ $L_1 = +0.6 \times 10^{-7}$ cm^{-2}

$K_2 = 0.97$ $L_2 = -0.5 \times 10^{-7}$ cm^{-2}

For HPD 2: $K_1 = 1.1$ $L_1 = +0.3 \times 10^{-7}$ cm^{-2}

$K_2 = 1.0$ $L_2 = -0.6 \times 10^{-7}$ cm^{-2} .

Finally, we compare the results of HPD 1 with those of HPD 2. In this case the view-averaged curvature obtained with each machine is used. This quantity is defined for each roll as

$$\langle \rho_0^{-1} \rangle = 1/3 \left[\rho_0^{-1} \text{ (V1)} + \rho_0^{-1} \text{ (V2)} + \rho_0^{-1} \text{ (V3)} \right]$$

and is given in Table 5 and plotted in Fig. 4e. The regression line is

$$\langle \rho_0^{-1} \rangle_{\text{HPD2}} = 1.07 \, \langle \rho_0^{-1} \rangle_{\text{HPD1}} - 2.3 \times 10^{-6} \text{ cm}^{-1} .$$

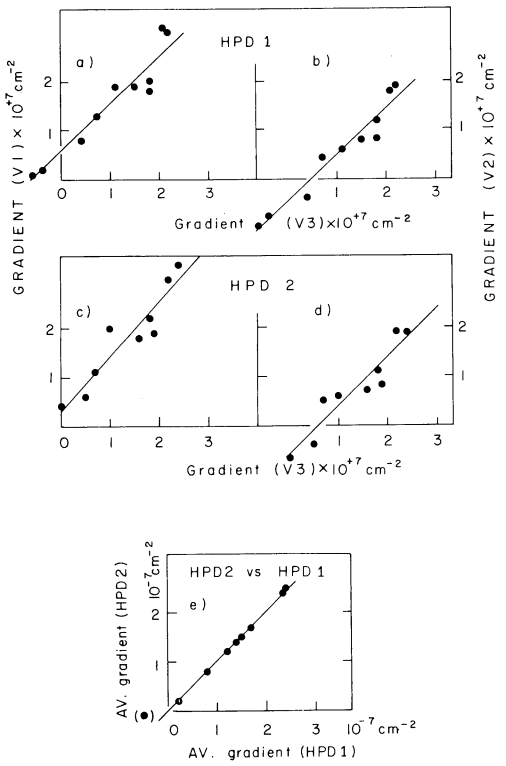

Fig. 5

Curvature gradients in the y-direction in various views and rolls, measured on two HPD's. Inter-view regressions shown for

a) view 1 versus view 3 on HPD 1,
b) view 2 versus view 3 on HPD 1,
c) view 1 versus view 3 on HPD 2,
d) view 2 versus view 3 on HPD 2,

and comparison of the two measuring machines in e) using view-averaged curvatures gradients.

The discrepancy between the two measuring machines corresponds to a film plane shift of about 5 μm in the sagitta of all tracks in all views. The curvature gradients treated in a similar manner (Table 5 and Fig. 5e) yield

$$\left\langle \frac{d\rho_0^{-1}}{dy} \right\rangle_{HPD2} = 1.0 \left\langle \frac{d\rho_0^{-1}}{dy} \right\rangle_{HPD1} ,$$

where in both cases the point for EM-06 is given the weight zero as it seems to deviate more than normal.

The observed average curvatures vary in the set of rolls from about 0 to 9 × 10^{-6} cm^{-1}, which is significantly outside the range of random fluctuations. A corresponding statement holds for curvature gradients. The important observation is that the slopes of the regression lines are close to unity. This means that the systematic curvatures are viewed in about the same way by all three cameras, and reproduce fairly well when remeasured on another measuring machine (roll EM-06 on HPD 2 seems more than normally disturbed, however). It is therefore reasonable to conclude that the main cause for these spurious curvatures lies inside the chamber and that they do not originate in the optics, the film, the measuring machines, or in reconstruction inaccuracies. However, influences from these sources could be responsible for deviations from the perfect case with slopes equal to unity and intercepts equal to zero. It remains to find out whether it is bulk liquid motion which distorts the tracks or thermal turbulence which distorts the track images. The dependence on flash time

delay provides the clue to the answer. The view-averaged curvatures as given in Table 5 are plotted against flash delay in Fig. 6 with separate symbols for the three sets of early, symmetric, and late exposure conditions. The rapid rate of increase of the curvatures for the late exposures is in itself a clear indication that bulk liquid motion acts in such a way as to distort the tracks. An extrapolation to zero flash delay gives a quite small curvature consistent with those valid for the early set, which are rather independent of the flash delay. The symmetric case falls in between the other two sets. The lines drawn in Fig. 6 are to guide the eye and to indicate the possibility of a common extrapolated value at zero flash delay. This value should ideally be zero. It seems to be small but different from zero. It could represent an uncorrected film distortion or optical distortion. In Fig. 7 the curvature gradients are plotted as a function of flash delay. They show much the same behaviour as do the curvatures themselves. The magnitudes are such that the curvatures at the physical bottom of the chamber, obtained by extrapolation*) to y = -30 cm are all small and consistent with zero contribution from liquid motion. This result makes us confident enough to conclude that bulk liquid motion exists and is the main cause of the larger curvatures and gradients.

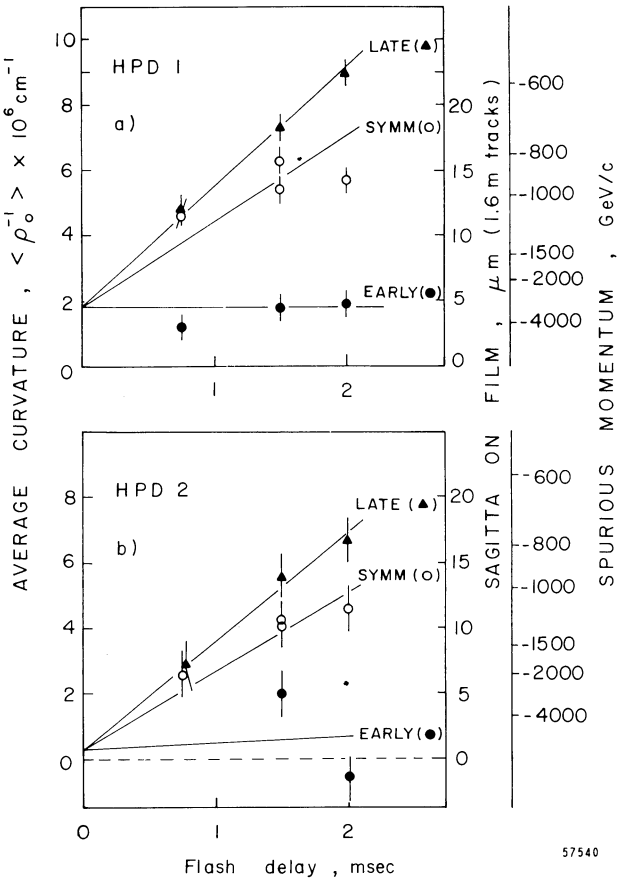

Fig. 6

Spurious curvatures versus flash delay with separate symbols for the EARLY (●), SYMMETRIC (○), and LATE (▲) set of exposures:

a) view-averaged central curvatures as measured on HPD 1;
b) view-averaged central curvatures as measured on HPD 2.

Scales to the right give the corresponding sagitta on film for 1.6 m long tracks and the spurious momentum in a magnetic field of 1.74 T, respectively. The lines are drawn to guide the eye.

*) $(\rho^{-1})_{BOTTOM} = \rho_0^{-1} - 30 \frac{d\rho^{-1}}{dy}$

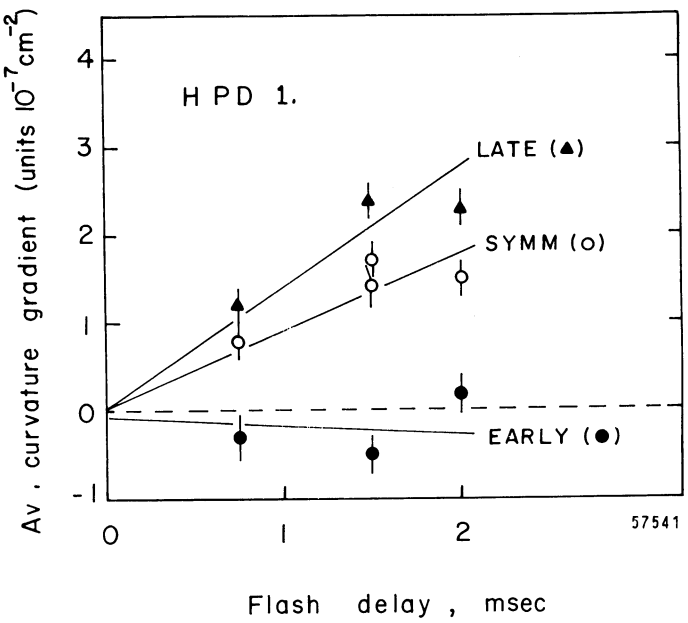

Fig. 7

The average curvature gradients versus flash time delay with separate symbols for the EARLY (●), SYMMETRIC (O), and LATE (▲) set of exposures.

In Fig. 6 separate scales show the sagittas in the film plane and the spurious momentum (p_0) in a field of usual strength (B = 1.74 T). Under normal conditions (symmetric exposure with a flash delay of 1.2 msec) the systematic displacement Δp in the momentum of a non-dipping track in the centre of the chamber would then be given approximately by

$$\frac{\Delta p}{p} = -\frac{p}{p_0} = +\frac{p}{1300} \qquad (p \text{ in GeV/c})$$

(a 16 GeV/c track would give Δp = +200 MeV/c).

The sign is such as to yield a measured beam momentum that is slightly higher than the nominal value under normal running conditions, i.e. with beam tracks curving down as they enter the chamber.

The relative liquid velocities between the centre and the ends of these 1.6 m long tracks is then about 15 cm/sec for the late set of exposures, and almost zero for the early set with the symmetric set in between. As an explanation of the observations, one could think of two superimposed motions. One of these could be a rather steady stirring of the liquid, downwards in the centre and upwards at the entry and exit ends. The other motion is a rapidly changing one which follows the piston movements. In the case of the early exposures, the two superimposed motions tend to cancel each other, while after the pressure minimum the two motions add to each other. Our data are not sufficient to test such a model in detail. The important observation is that spurious curvatures are smallest when beam and flash are positioned just before the pressure minimum (the early set of exposures), and they are then rather independent of flash time delay. As the gradients are also small under the early conditions, the statement holds true at all heights (y).

In high-energy experiments where spurious curvatures are suspected, one could determine the liquid motion part independently by plotting average values of (1/p) for beam tracks at a given height (y) versus y. The value extrapolated to y = -30 cm (the chamber bottom) should

then correspond to the nominal beam momentum. Some care has, of course, to be exercised in case a momentum dispersion of the beam exists in the y-direction.

Before concluding this section on systematic errors it should be noted that the parabolic fit discussed so far does not absorb all systematic errors. The corrected mean track profiles (parabolic effects subtracted out) show some wriggles. The amplitude of these are significantly different from zero in some x-regions. However, they are small and do not show the same regularities as the curvatures. Similarities between views and measuring machines indicate that they partly arise in the liquid. The maximum deviations are about ±2 μm in the film plane and thus about ±30 μm in space. In more detail, roll by roll and view by view, the maximum positive amplitudes are in the range +0.8 μm to +5.5 μm, and the largest negative amplitudes are in the range -0.7 μm to -2.6 μm. The average values are +2 μm and -1.5 μm, respectively. One maximum often repeats at the x-coordinate x = +25 cm. Under optimized running conditions (i.e. early beam and flash) these errors are the only systematic ones which can be associated with track distortions due to the chamber liquid.

Our conclusion is then that the CERN 2 m deuterium chamber could eventually be capable of a precision of 30 μm in space. However, before this statement can be accepted one must show that no larger random errors occur associated with the liquid motions or turbulences. Such errors, if they exist, would influence the momentum of a single track. As will be seen in the next section on random errors, even this type of error is very small.

7. RANDOM ERRORS

Two types of random errors are generally considered in bubble chamber work, namely the setting error of measurements and the error due to multiple Coulomb scattering. The first type is usually treated as a constant which is characteristic of the measuring procedure. It is conceivable that a third random component could exist associated with the liquid motion. So far we have studied the average curvatures and will now consider the scatter of individual curvatures around the average values. We will consider three random error components in the curvature parameter c, or equivalently in ρ^{-1} ($c = 1/M2\rho$, where M = 13.1 is the magnification factor). Let us denote the standard deviations of the three components:

(1) σ_M , due to multiple scattering;

(2) σ_F , due to setting error and other view-dependent errors;

(3) σ_L , due to variations in the liquid motion.

The components (1) and (3) should be seen in all three views to be highly correlated, whereas by definition the second component is uncorrelated between views. Thus we can write, for the curvature variances and covariances:

$$\text{view 1 :} \quad \sigma^2(1) = \sigma_M^2 + \sigma_L^2 + \sigma_{F1}^2$$

$$\text{view 2 :} \quad \sigma^2(2) = \sigma_M^2 + \sigma_L^2 + \sigma_{F2}^2$$

$$\text{view 3 :} \quad \sigma^2(3) = \sigma_M^2 + \sigma_L^2 + \sigma_{F3}^2$$

$$\text{view pairs :} \quad \text{cov}\,(\rho_\alpha^{-1}, \rho_\beta^{-1}) = \sigma_M^2 + \sigma_L^2 \qquad (\text{view } \alpha \text{ and view } \beta) \ ,$$

with $\alpha,\beta \in 1,2,3$ and $\alpha \neq \beta$.

The expectation value of σ_M is given by multiple scattering theory. As described in the Appendix we estimate the following values

$$\text{var } (\rho^{-1}) \equiv \sigma_M^2 = 6.11 \times 10^{-12} \text{ cm}^{-2}$$

$$\text{and} \qquad \sigma_M = 2.47 \times 10^{-6} \text{ cm}^{-1} .$$

Table 6 and Fig. 8 contain the observed values for different rolls, different views, and with both measuring machines (HPD 1 and HPD 2). We note that the inter-view correlation coefficients are high, about 0.8. The observed values of the covariances are in general in good agreement with the expectation from multiple scattering alone. The over-all average is $(6.6 \pm 0.1) \times 10^{-12}$ cm^{-2}, whereas the multiple scattering expectation is $(6.1 \pm 0.6) \times 10^{-12}$ cm^{-2}. This means that there is not much room for a liquid motion component. The above difference gives $\sigma_L \approx 0.7 \times 10^{-6}$ cm^{-1} which corresponds to a random sagitta error of about 25 μm in chamber space. Multiple scattering on 16 GeV/c tracks obviously dominates the random errors, and therefore only an order of magnitude can be given to the component associated with liquid motion.

Table 6

Curvature random errors

Roll	HPD	Standard deviation [a] of $\rho^{-1} \times 10^6$ cm^{-1}			Correlation coefficients [b] for view pairs			Covariance [c] of curvatures $\times 10^{12}$ cm^{-2}		
		View 1	View 2	View 3	(12)	(23)	(31)	View (1,2)	View (2,3)	View (3,1)
ES-05	1	2.5	2.9	2.5	0.74	0.75	0.80	5.4	5.4	5.0
EM-06	1	2.9	3.3	2.8	0.78	0.81	0.88	7.5	7.4	7.1
EL-07	1	2.7	3.0	2.6	0.84	0.85	0.89	6.7	6.6	6.1
SS-04	1	2.7	3.3	2.7	0.77	0.77	0.87	6.8	6.6	6.3
SM-02	1	2.8	3.5	2.9	0.74	0.78	0.85	7.3	8.1	6.9
SM-11	1	2.8	3.1	2.7	0.82	0.84	0.88	7.0	6.9	6.6
SL-03	1	2.7	3.4	2.9	0.74	0.74	0.86	6.7	7.4	6.6
LS-08	1	2.5	2.6	2.6	0.81	0.81	0.82	5.3	5.5	5.3
LM-09	1	2.9	3.1	2.9	0.79	0.78	0.88	7.1	7.0	7.4
LL-10	1	2.6	2.9	2.6	0.82	0.82	0.85	6.2	6.2	5.7
EM-06	2	2.8	3.3	3.1	0.80	0.75	0.80	7.3	7.6	7.0
EL-07	2	2.7	3.0	2.7	0.81	0.83	0.89	6.5	6.6	6.5
SS-04	2	2.7	3.2	2.6	0.75	0.75	0.87	6.4	6.3	6.0
SM-02	2	2.7	3.5	2.9	0.78	0.79	0.87	7.4	8.0	6.9
SM-11	2	2.6	2.9	2.6	0.84	0.86	0.90	6.3	6.6	6.0
SL-03	2	2.8	3.3	2.9	0.75	0.76	0.87	6.9	7.2	7.1
LS-08	2	2.6	2.8	2.5	0.82	0.80	0.81	5.9	5.6	5.3
LM-09	2	2.8	3.2	2.9	0.81	0.78	0.88	7.2	7.7	7.1
LL-10	2	2.6	3.2	2.5	0.85	0.83	0.89	7.1	6.7	5.9

a) Error: $\pm 0.10 \times 10^{-6}$ cm^{-1}

b) Error: ±0.02

c) Error: $\pm 0.3 \times 10^{-12}$ cm^{-2}

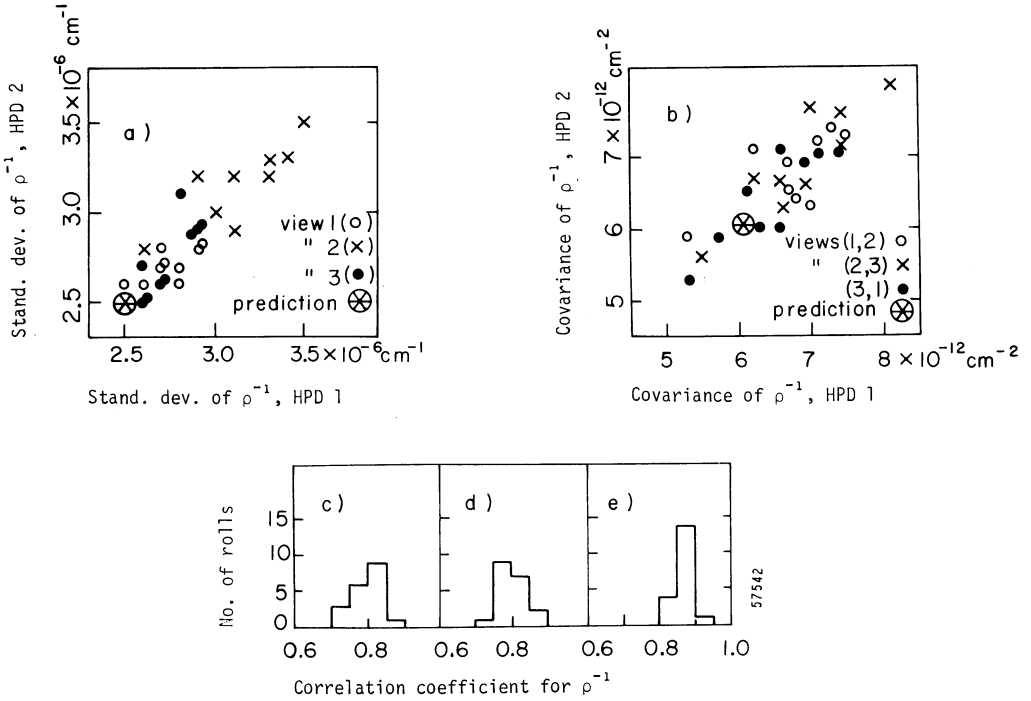

Fig. 8 Random curvature errors as given in Table 6.

a) Standard deviations of the curvature distributions in various views and rolls. Estimated error on each point is 0.1×10^{-6} cm^{-1};

b) covariances of the curvature distributions. Estimated error on each point is 0.3×10^{-12} cm^{-2} [the prediction from multiple scattering theory is shown in (a) and (b)]

c) correlation coefficients of curvatures in view 1 and view 2;

d) correlation coefficients of curvatures in view 2 and view 3;

e) correlation coefficients of curvatures in view 3 and view 1.

Turning now to the standard deviations of the curvatures view by view and roll by roll in Table 6 and Fig. 8, we note that the values are somewhat larger than what is expected from multiple scattering. Particularly high values are obtained in view 2. The average values for all rolls are:

$$\text{view 1} : \sigma(1) = 2.70 \times 10^{-6}\ \text{cm}^{-1} \pm 0.03 \times 10^{-6}\ \text{cm}^{-1}$$

$$\text{view 2} : \sigma(2) = 3.12 \times 10^{-6}\ \text{cm}^{-1} \pm 0.05 \times 10^{-6}\ \text{cm}^{-1}$$

$$\text{view 3} : \sigma(3) = 2.74 \times 10^{-6}\ \text{cm}^{-1} \pm 0.03 \times 10^{-6}\ \text{cm}^{-1} .$$

Using the average value of the covariance, we obtain for the average view-errors σ_F:

$$\sigma_F(\text{view 1}) = (0.8 \pm 0.1) \times 10^{-6}\ \text{cm}^{-1}$$

$$\sigma_F(\text{view 2}) = (1.8 \pm 0.1) \times 10^{-6}\ \text{cm}^{-1}$$

$$\sigma_F(\text{view 3}) = (0.9 \pm 0.1) \times 10^{-6}\ \text{cm}^{-1} .$$

The contribution from setting errors (about 2 μm) should be substantially smaller than the above for a 50-point track, namely 0.4×10^{-6} cm^{-1}. We will show later that it would be unreasonable to assume increased setting errors. After subtraction of the setting error contribution the remaining error is, when referred to the film plane as a sagitta error:

view 1 : sagitta error = 1.8 μm

view 2 : sagitta error = 4.4 μm

view 3 : sagitta error = 2.0 μm .

It seems reasonable to associate this error with the fact that acetate-backed film is lacking in rigidity and that the above values represent the limiting error which cannot be removed by increasing the number of measured points. As these errors are uncorrelated between views, their combined effect corresponds to a sagitta error of 1.7 μm on film or 22 μm in space. The fact that view 2 consistently gives higher values indicates that at least part of the effect arises in the cameras or in the development of the film.

It is informative to study the random part of straight line residuals in some detail. At each fixed x-coordinate along the tracks, the residuals r(x) in a sample of tracks are expected to be normally distributed with the profile values $\bar{r}(x)$ as mean and a certain standard deviation. Both quantities vary with x. There are at least two contributions to the standard error. One is the constant setting error ε. The other is the multiple scattering component which should strongly depend on x. The detailed theory[5] shows that the residual distribution is widest at the two ends of the tracks, that quite narrow distributions exist at about 20% of the track length, and that in the centre region it is wider again. For the present application to a large number of equidistant points, the following formula (see Ref. 5) holds for the variance of the residual distributions:

$$\text{var } r(x) = KL^3(p\beta c)^{-2}\left[\frac{1}{640} - \frac{37}{1120}\left(\frac{x}{L} - \frac{1}{2}\right)^2 + \frac{5}{24}\left(\frac{x}{L} - \frac{1}{2}\right)^4 - \frac{1}{10}\left(\frac{x}{L} - \frac{1}{2}\right)^6\right],$$

where in our case $K = 0.357$ MeV^2 cm^{-1} (see Appendix), $p\beta c = 16$ GeV, and $L = 163$ cm.

In the above formula x should be zero at one end of the track and x = L at the other end. Because the sample is described in chamber space with x equal to chamber coordinates, and since neither the first point nor the last one occurs at exactly the same x-coordinate for all tracks, the above formula has been folded with the end-point distributions. This is a minor correction which, however, improves the agreement with the observations. The only parameter adjusted to fit the data in the regions of the two minima is the setting error ε. This is taken as an x-independent constant. Figure 9 gives some of the many curves obtained (one for each roll and view and subsample UP, MID, and LOW). The curves in Fig. 9 agree fairly well with expectation. Again we see that multiple scattering dominates the errors at the ends and in the middle of the tracks. The two minima are, however, very sensitive to the size of the setting error. The error refers to HPD master points, representing the average position of many (about 40) near-by bubble diffraction images. A large number of setting errors have been obtained. In a given roll, good agreement holds between views,

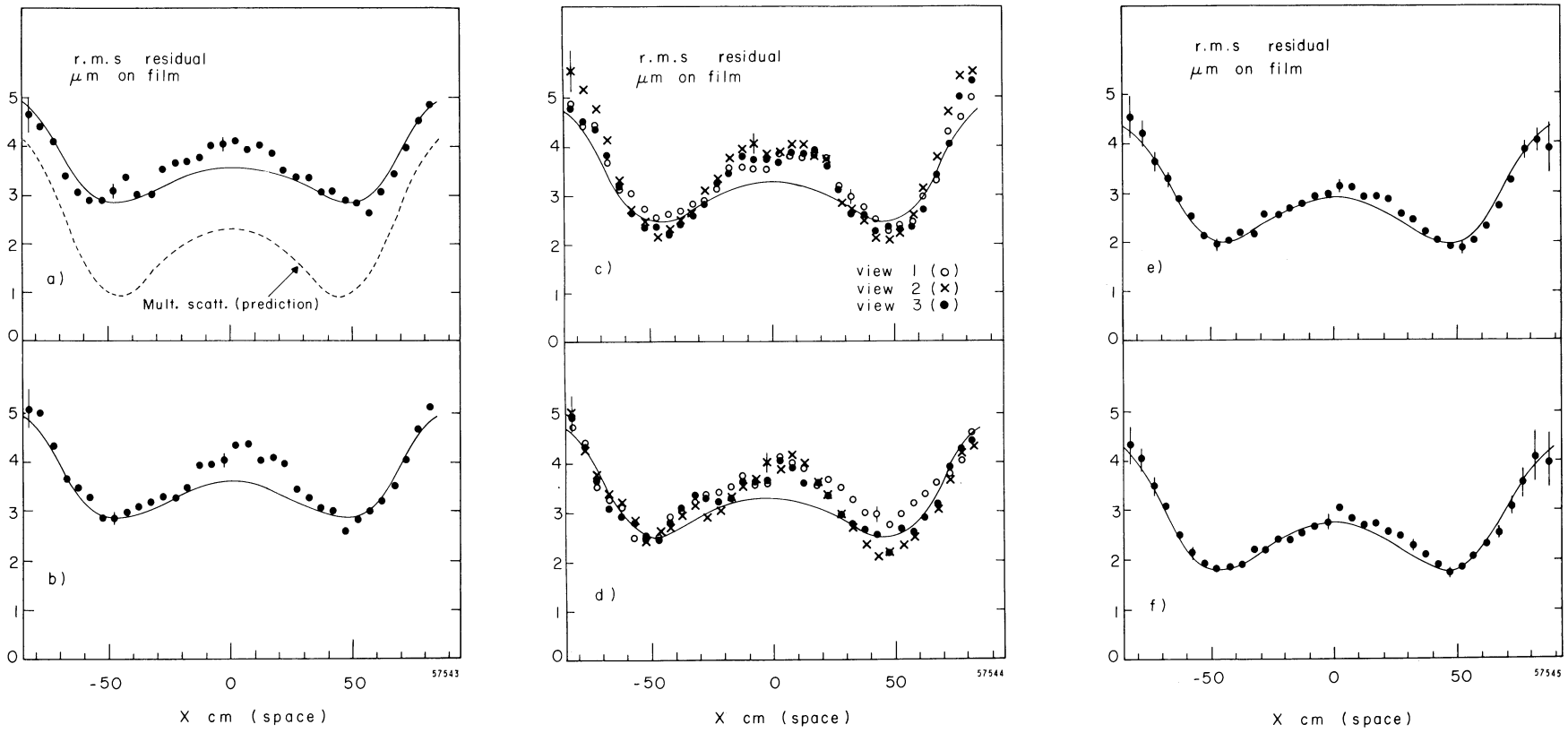

Fig. 9 The standard deviation of the residuals of a sample of beam tracks taken at fixed x-intervals along the beam direction as of function of x (D_2-run). The curves are calculated from the theory of multiple Coulomb scattering with a setting error quadratically added. The dotted curve gives the contribution from multiple scattering alone:

a) late with 2.0 msec flash delay, middle sample, view 1, ε = 2.7 μm

b) symmetric with 2.0 msec flash delay, low sample, view 3, ε = 2.7 μm

c) symmetric with 1.5 msec flash delay, low sample, all views, ε = 2.3 μm

d) symmetric with 1.5 msec flash delay, upper sample, all views, ε = 2.3 μm

e) early with 0.8 msec flash delay, middle sample, view average, ε = 1.8 μm

f) late with 0.8 msec flash delay, middle sample, view average, ε = 1.6 μm

HPD's, and subsamples (UP, MID, and LOW). Roll-to-roll variations exist, however. As shown in Fig. 10, the results indicate that the setting error increases with flash delay. We could interpret this effect in a variety of ways. In Fig. 10b a quadratic addition of a setting error ε_0 together with a component due to the increase in bubble size $\alpha\sqrt{\tau}$ is tried. However, such a hypothesis leads to too small an ε_0 and would require very large bubble size variations, especially when one considers that each HPD master is an average over many bubbles. We could also interpret the effect as being due to a fluctuating velocity component of thermal eddies. In this case, one would quadratically add ε_0 and $\bar{\nu}\cdot\tau$, where $\bar{\nu}$ is the r.m.s. velocity demagnified to the film plane. Under this hypothesis we find $\varepsilon_0 \approx 1.3$ μm and $\bar{\nu} = 1.2$ μm/msec. Magnifying to space and with the assumption that each master point covers a few eddies ($\sim$ 4 to 8), we find the r.m.s. velocity of the eddies to be about 4 cm/sec. Whatever the interpretation is, the increase of this error with flash time delay is real, and thus the concept of the setting error as a constant machine parameter might not always be applicable.

One may ask to what extent the earlier-found film sagitta errors -- especially large in view 2 -- are noticeable in the residual variance curves at present being studied. In the presence of the rather large multiple scattering errors, a sagitta error of only 2 μm is difficult to detect. However, an effort has been made to confirm the earlier result that view 2 shows a larger film noise sagitta. To this end the x-dependence of the variance ratios between views has been studied. It turns out that as expected the view 2 variance is, on the average, significantly larger than the variances of the other views near the entry and exit ends of the track sample. For $|x| > 65$ cm the mean variance ratios are found to be 1.19 ± 0.02 (view 2/view 1), 1.17 ± 0.02 (view 2/view 3), and 1.01 ± 0.01 (view 1/view 3). Since this region is sensitive to a parabolic film noise error, we conclude that the larger film noise in view 2 has been confirmed. The effect is not due to a larger setting error.

Finally, we comment on the small disagreements between the data points and the curves in Fig. 9. Some extra noise near the centre of the chamber is seen, and occasionally also near the ends. These three regions are very sensitive to the inclusion of tracks with single or plural scattering. Empirically, we found that a few per cent of such tracks can have dramatic effects on the residual variances. Although such tracks have been eliminated by

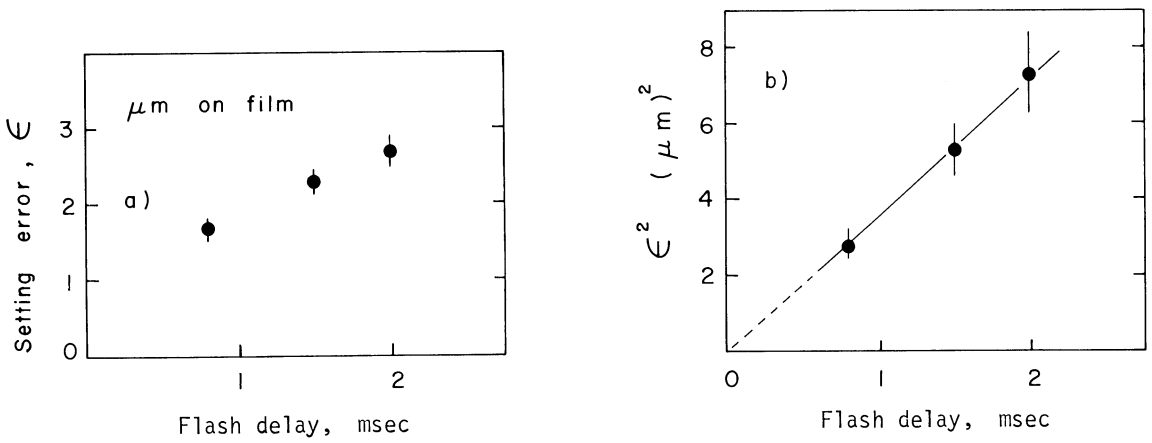

Fig. 10 The setting error (ε) in dependence of the flash delay:
a) linear scale
b) quadratic scale in ε.

the methods described in Section 5.3, any further analysis has to be made with caution*). The disturbances near the chamber centre seen in Fig. 9 can therefore be said to correspond to an additional noise of less than 30 μm in space. This noise could be related to the liquid noise in the curvatures considered before, namely $\sigma_L(\rho^{-1}) \approx 0.7 \times 10^{-6}$ cm^{-1}. Both observations give about the same noise value of the order of 25 to 30 μm in space. Considering the size of multiple scattering of 16 GeV/c pions, not much more can be said about the liquid noise error. The fact that the random error component is dominated by multiple scattering effects is in itself a demonstration of how precise the chamber is, and also of the stability of the measuring system.

8. CONCLUSIONS

1) Bulk liquid motions exist, which vary with timing conditions relative to the pressure curve.

2) In the worst conditions of the series of runs (beam at pressure minimum and 2 msec flash delay) the motion gives rise to a sagitta of about 300 μm in space at the chamber centre and even more closer to the piston. The corresponding spurious momentum is about -800 GeV/c.

3) Optimum timing conditions exist when beam arrival is about 2 msec before the pressure minimum.

4) Under optimum conditions the remaining sagitta is small (about 3 μm on film). The remaining spurious momentum is $|p_0| > 3000$ GeV/c.

5) The errors in the liquid have been estimated in several ways (all given in chamber space):
   - i) from systematic profile differences, from parabolic shapes (wriggles) with amplitudes about 30 μm;
   - ii) from curvature covariances: $\sim$ 25 μm (sagitta);
   - iii) from straight line residual variances: $<$ 30 μm;
   - iv) from setting error increase with flash delay: $\sim$ 25 μm (at 1.2 msec).

Errors (ii) and (iii) are probably related.

By addition of an r.m.s. average of 20 μm due to the irregular component (i) and another average of about 25 μm from (iii) with (iv), we find that the resulting single-point standard deviation under optimum conditions is about 40 μm in chamber space.

The lack of film rigidity seems to set a limit on the measuring accuracy of curvatures. When many points are placed on tracks, this error becomes more important than the setting error. Combined with the chamber errors (i) and (iii) the minimum standard error of the sagitta on 1.6 m long tracks is then about 40 μm in space. A systematic error of unknown origin of the same magnitude seems difficult to avoid (see point 4 above).

---

*) On the hypothesis that the only random errors are those due to a setting error ε and the multiple scattering, both ε and the scattering constant K can be obtained from fits to the data. A set of 27 curves such as those in Fig. 9 gave the average $K_{fit} = (0.91 \pm 0.05)K_{comp}$, and setting errors increased by about 15% over those given in Fig. 10. However, the fits are not very good, and we believe the hypothesis to be wrong. Although the above errors are dominating the straight line residuals, they are probably not the only ones present.

CHAPTER II

TESTS IN A HYDROGEN-FILLED CHAMBER

G. Ekspong and J. Zoll

The test results obtained in the run with the hydrogen-filled chamber are summarized in this chapter. The method used to analyse the data is much the same as in the deuterium case.

1. THE EXPOSURES AND MEASUREMENTS

A series of four runs were made with the beam arrival time 2 msec before the chamber pressure minimum and the following flash delay times: 0.8, 1.2, 1.6, and 2.0 msec. These early runs are denoted by E 0.8, E 1.2, E 1.6, and E 2.0. Four runs under symmetric conditions are denoted by S 0.8, S 1.2, S 1.6, and S 2.0. Finally, late runs were made with the same four flash delay times and a flash time fixed at 2 msec after the pressure minimum (L 0.8, L 1.2, L 1.6, and L 2.0).

Two special tests were made under symmetric conditions with the normal flash delay of 1.2 msec. The cooling loop around the piston head was kept cooler than normal. The idea was to see if cold liquid would be shot down into the visible region of the chamber. If so, the images of the bubbles would be displaced owing to local variations in the index of refraction in the liquid. No such effects could be seen in the track profile curves or in any other parameter. The temperature of this cooling loop (LOOP 2) is then not critical.

The time of beam arrival was measured with a new electronic device. Calibration tests showed the zero point of this device to be shifted by 0.4 msec from the pressure minimum. Here, all times are corrected for this shift and are given relative to the pressure minimum, as seen on the oscilloscope in the chamber control room.

The data are of still higher quality than in the deuterium runs. The following are the changes:

i) The camera port windows are new and of much improved optical quality.

ii) The beam was chosen to be 24 GeV/c protons (rather than 16 GeV/c pions as in the D_2 run). The multiple Coulomb effects are thus reduced and other errors are seen more easily. The scattering constant is calculated from theory to be $K = 0.314$ MeV^2 cm^{-1}. The chamber pressure was 4.85 to 4.84, the temperature 4.10 to 4.09, and the pressure drop about 3.0 (all in kg/cm^2).

iii) The information on the position of the plane 2 fiducial marks was kept on the Geometry output tape. This was later used to refit a parabolic distortion term ($\alpha_4 \times x^2$) to each frame individually and to correct the residuals. This procedure improved the quality of the data in two respects:

a) it removed systematic distortions in some rolls and views where the average α_4 was different from that in the over-all set of films;

b) it reduced the random component of film curvature which is small but clearly present.

iv) Only HPD2 (now readjusted with its earlier film distortion removed) was used for the measurements.

The optical constants, determined by the program PYTHON, are given in Table 7 and the distortion parameters in Table 8. It is to be noted that the values of the α_4-parameter given there was later redetermined frame by frame.

Table 7

Optical constants for the hydrogen tests

Camera	Camera positions (cm)			Media properties	
	x	y	z	Index	Thickness (cm)
1	13.1637	28.9864	241.9767	1.0000	217.4889
2	-31.8360	-0.0034	242.1454	1.5259	7.4600 (V1) 7.4990 (V2) 7.4980 (V3)
3	13.1629	-28.9942	242.1159	1.5324	17.0278
				1.1005	50.5400

Table 8

Distortion parameters used in track reconstruction (H_2)

Camera	x-tilt parameter α_1	y-tilt parameter α_2	Lens distortion parameter α_3	Parabolic parameter α_4
1	-0.00059	-0.00136	-0.00447	0.00108
2	-0.00093	-0.00088	-0.00539	0.00015
3	-0.00127	0.00036	-0.00462	-0.00055

2. THE QUALITY OF THE DATA AND PROFILE RESULTS

A striking feature of the new data is their high quality. If one studies the mean track profiles one finds the following regularities:

View 1 and view 3 agree in detail to better than ±0.5 μm at all x-values (Fig. 11). It is to be noted that this level of agreement could be obtained only after fitting α_4 for every frame and view.

View 2 differs in a reproducible way from the other two views, as seen on Fig. 11. The 14 different samples give the same curve to ±0.25 μm, which has an amplitude of about 1.5 μm on the film.

Another small disagreement between views (here eliminated) is a linear translation and rotation of the residuals. However, view 1 and view 3 agree on the average in each of the 14 different runs to within a fraction of 1 μm, whereas view 2 exhibits a shift of about 2 μm and also a rotation of about 0.02 mrad relative to the other two views. The shift has a tendency to increase with bubble size (i.e. flash time delay) and the effect could be caused by the dark field illumination effect on bubbles of finite size.

Ideally, the average residual at each x-value should be zero. The systematic deviations give the mean track profiles shown in Fig. 12 for the different timing conditions. As seen from the curves, the early timing conditions (except with 2 msec flash delay) represent the optimum results. The data are from view 1 and from the middle part (near y = 0) of the chamber. Each point has a statistical error of about ±0.3 μm on film.

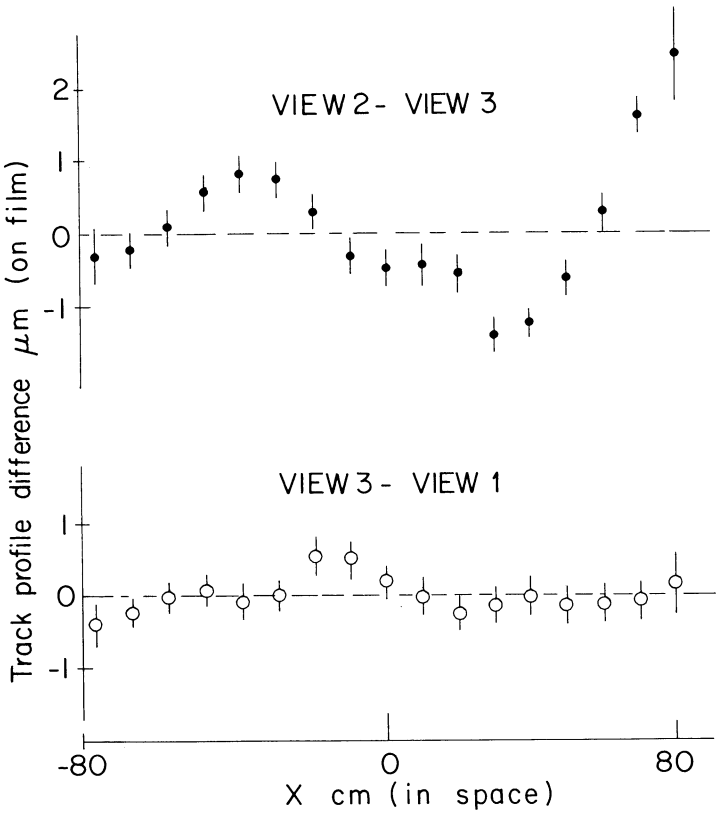

Fig. 11

The difference between track profiles in the hydrogen runs.

a) View 2 - view 3 difference, showing some uncorrected effect of 1 to 2 μm on the film plane.

b) View 3 - view 1 difference, showing very good agreement. The error bars are standard deviations in the sample of 14 runs.

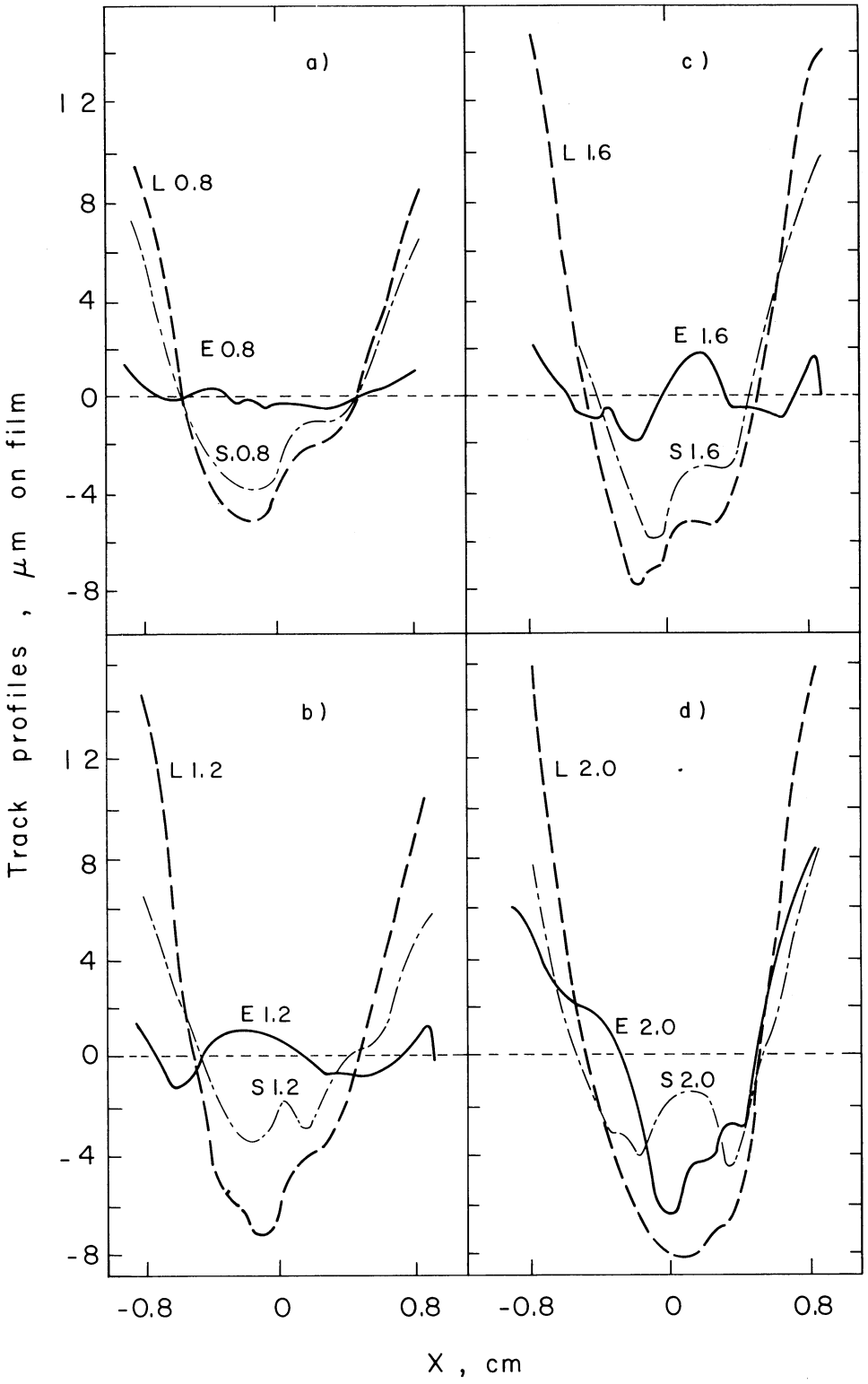

Fig. 12 Track profiles in hydrogen for the middle sub-samples at various flash-delays (0.8, 1.2, 1.6, 2.0 msec) and beam-arrival times: E for early, S for symmetric, L for late. The profiles are shown as hand-drawn lines through the points obtained for 5 cm intervals; each such point has a statistical error of ±0.3 μm on film.

3. SYSTEMATIC ERRORS (SPURIOUS CURVATURES)

The main results as regards the systematic errors are collected in Table 9, which contains the average curvature of the tracks (magnified to chamber space). The agreement between the three views is seen to be very good and suggests standard errors of less than 0.2×10^{-6} cm^{-1} in the average curvature ρ_0^{-1} in each view consistent with the purely statistical error of 0.15×10^{-6} cm^{-1}. The table also contains the curvature gradients, which agree within $\pm 0.1 \times 10^{-7}$ cm^{-2}. The data are highly consistent and one finds the best agreement between views 1 and 3. For view 2 the curvatures are slightly larger, by 0.5×10^{-6} cm^{-1}, and the gradients are larger by 0.3×10^{-7} cm^{-2}. In the following, the values obtained as the average between the three views are used. The dependence on timing conditions are given in Figs. 13 and 14, obviously showing the same behaviour as the results from the deuterium runs (see Figs. 6 and 7). The "EARLY" timing conditions, except with 2 msec flash delay, give the least curvatures, the "LATE" ones the largest, while the "SYMMETRIC" ones are in between. Again an interpretation with two super-imposed liquid motions seems natural; one movement which represents a stirring of the liquid down in the centre (under the piston) and upwards near the beam entry and exit ends of the chamber, the other movement following

Table 9

Systematic errors.
Spurious curvatures of no-field tracks in the CERN 2 m HBC.
ρ_0^{-1} = curvature at the centre (y = 0) in units of 10^{-6} cm^{-1};
$d\rho^{-1}/dy$ = curvature gradient in units of 10^{-7} cm^{-2}.

Roll	Average curvature, ρ_0^{-1}				Curvature gradient, $d\rho^{-1}/dy$			
	View 1	View 2	View 3	All-view average	View 1	View 2	View 3	All-view average
E 0.8	-0.1	0.8	0.2	0.3	-0.7	-0.5	-0.7	-0.6
E 1.2	-0.6	0.2	-0.4	-0.3	-1.0	-0.5	-0.8	-0.8
E 1.6	0.2	0.3	0.0	0.2	-0.2	0.1	-0.2	-0.1
E 2.0	4.3	4.3	4.0	4.2	0.3	0.6	0.3	0.4
S 0.8	4.1	4.1	3.8	4.0	0.7	1.0	0.7	0.8
S 1.2	5.2	5.4	5.0	5.2	1.4	1.7	1.5	1.6
S 1.6	6.5	6.7	6.2	6.5	1.6	1.8	1.6	1.7
S 2.0	5.5	5.7	5.0	5.4	1.6	1.8	1.5	1.6
L 0.8	6.2	6.2	5.7	6.0	1.3	1.7	1.4	1.5
L 1.2	8.9	9.3	8.6	8.9	2.1	2.4	2.1	2.2
L 1.6	9.8	10.0	9.9	9.9	2.4	2.7	2.4	2.5
L 2.0	11.2	11.4	10.8	11.1	2.9	3.3	3.0	3.1
S 1.2 [a]	6.4	6.7	6.3	6.4	1.0	1.4	1.2	1.2
S 1.2 [b]	5.3	5.8	5.2	5.4	0.7	1.2	1.0	1.0

a) Loop 2 cooler than normal
b) Loop 2 still cooler

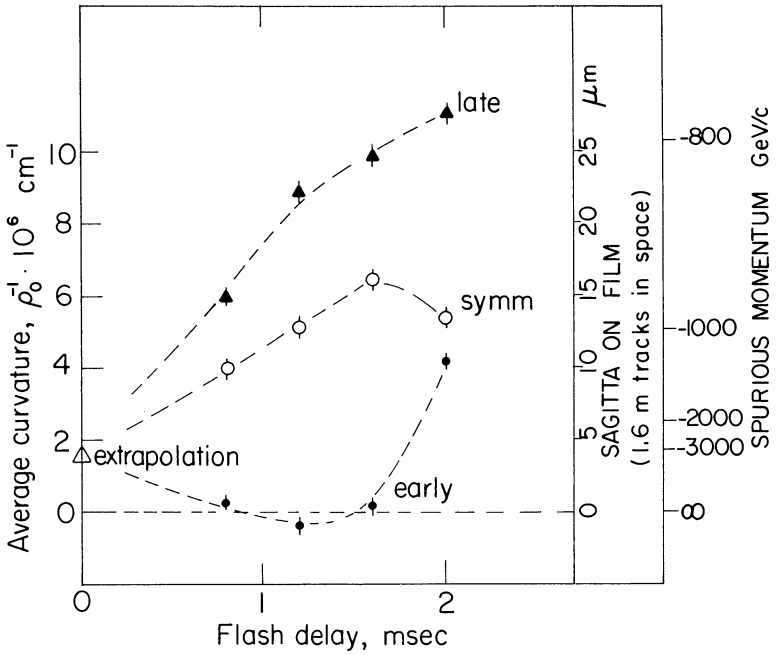

Fig. 13

The dependence on flash time delay of the average curvature in the hydrogen run (at y = 0). Separate scales show the spurious momentum (p_0) in a field of 1.74 T and the sagitta in the film plane on 1.6 metre long tracks.

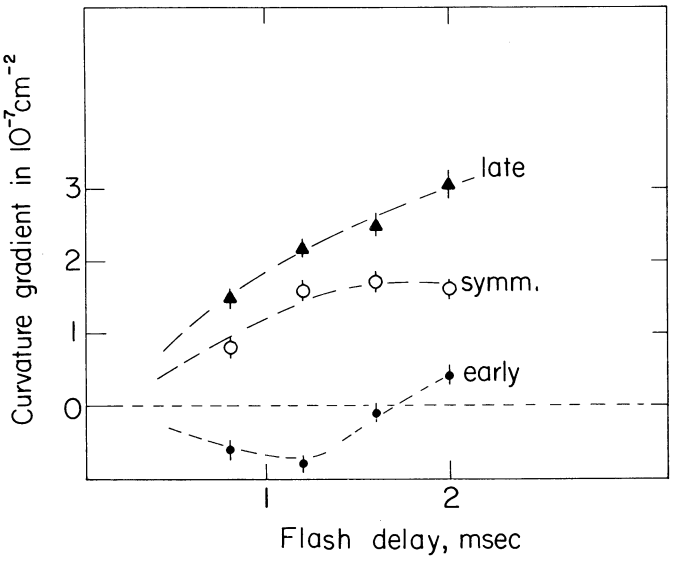

Fig. 14

The dependence on flash time delay of the average curvature gradients, $d\rho^{-1}/dy$ (H_2-run).

the piston faster in the centre than near the ends. The curvature gradient is such that near the physical bottom (y = -30 cm) almost no liquid motion is seen. However, the average extrapolated curvatures both in space ($y \to -30$ cm) and in time ($\tau \to 0$) is small but non-zero (see Fig. 13).

The systematic curvatures studied so far refer to fits over the entire visible region, about 1.6 metre. Local variations exist, which can give both smaller and larger effects. We give two examples chosen to be representative. In the first case, we choose symmetric conditions with 1.6 msec flash delay. In the second, the early condition with 1.6 msec flash delay. Since the systematic shift depends on how long the fitted track is, we have

chosen to simulate HPD measurements, which use the full length of the track from the entry to the apex. Plotted in Fig. 15(a,b) are the systematic errors $\Delta p/p$ for 10 GeV/c beam tracks as a function of the apex coordinate. For other momenta the result is proportional to the momentum p, since $\Delta p/p = p/p_0$ (where p_0 is the spurious momentum).

In Fig. 15(c,d) a simulation of spiral reader measurements is shown for which the measured track length is limited by the spiral arm and is chosen to be 65 cm. It is seen that local variations of p_0 exist in our data, which give rise to systematic shifts of varying magnitude. Under the usually used symmetric timing conditions and when measured on an HPD, the effect acts in a way as if the beam was accelerated by the chamber. The EARLY conditions are to be preferred.

If the liquid motion pattern should remain reproducible over periods as long as a whole run, then one could map these movements as in the above cases. For this, one should measure a few hundred no-field tracks and determine the mean track profile both before and after the run. A table of corrections to bubble image positions could be introduced before space reconstruction takes place. In this way, a new level of precision could eventually

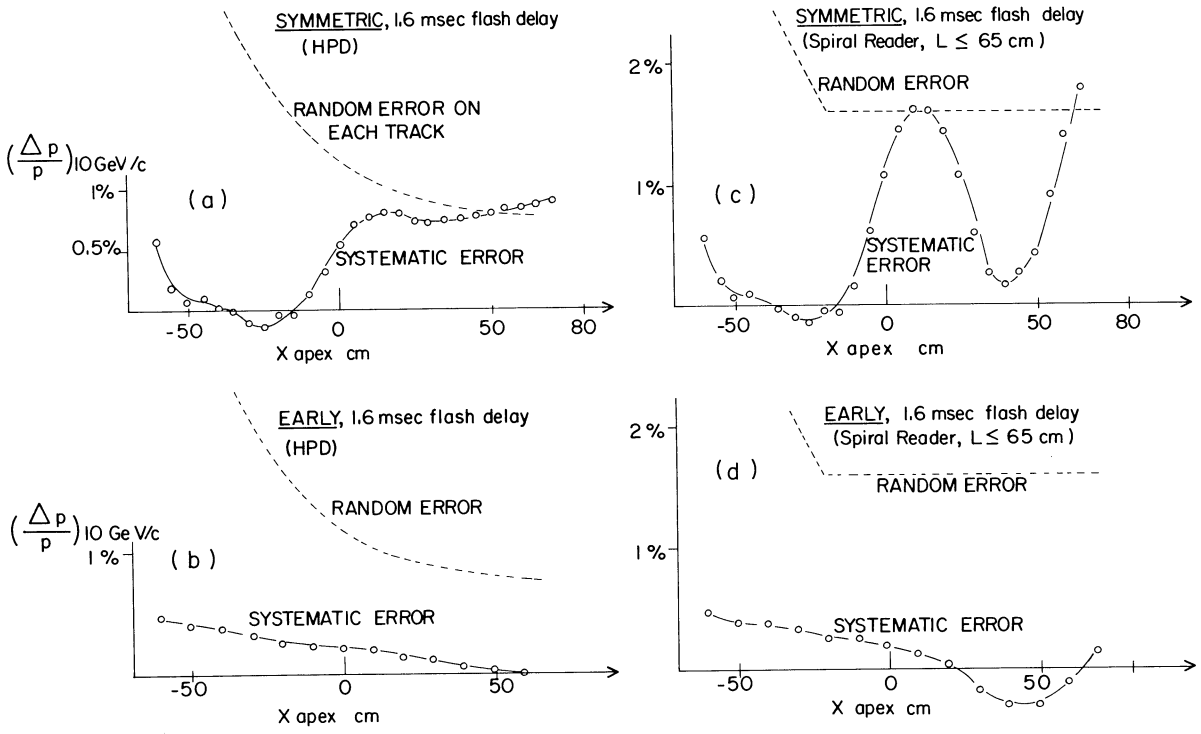

Fig. 15 Expected systematic shifts of beam momentum (Δp) in dependence of the apex coordinate, x_A. Calculations based on 10 GeV/c. The dotted curves show the magnitude of random errors, multiple scattering and a 40 μm setting error included.

a) HPD-simulation for the symmetric run with 1.6 msec flash delay. Note the spurious acceleration near the chamber centre.

b) HPD-simulation for the early run with 1.6 msec flash delay. A small spurious deceleration effect down to zero systematic error is seen.

c) The same as (a) but simulated for a spiral reader with track length limited to 65 cm (space).

d) Same as (b) but for a spiral reader.

be reached. The present tests did not last long enough to study the required reproducibility of the local variations. However, effects similar to the ones found here have been seen in an experiment with high statistics (private communication by J.B. Gay and B. Maréchal). In that case the systematic beam momentum shifts in certain x-regions of the chamber remained unchanged over long periods.

4. RANDOM ERRORS

As before, three components of random errors are assumed to contribute. From the distributions of the curvatures, the standard deviations in each view and the covariances between view-pairs were determined after removal of a few (3%) of the tracks which were situated in the tails of the distributions. The relevant information is collected in Table 10.

One sees that the correlation coefficient is high ($\simeq 0.8$). The covariances are the same within errors in all three combinations. However, variations with the timing conditions exist. We assign two error sources which contribute, namely multiple Coulomb scattering (σ_M) and random liquid motions (σ_L), thus covariance = $\sigma_M^2 + \sigma_L^2$.

Theoretically, we calculate $\sigma_M(1/\rho) = 1.56 \times 10^{-6}$ cm^{-1} and thus we expect the covariance $\geq 2.42 \times 10^{-12}$ cm^{-2}. The smallest values, 2.2×10^{-12} cm^{-2} and 2.5×10^{-12} cm^{-2}, agree with the limit. Most of the rolls require a contribution from random liquid motion. The derived values of σ_L lie in the range $0 < \sigma_L < 1.9 \times 10^{-6}$ cm^{-1} in ρ^{-1} or, expressed as the sagitta in space on 161 cm long tracks, $0 < s < 60$ μm. The average values are $\langle\sigma_L\rangle = 1.0 \times 10^{-6}$ cm^{-1} and $\langle s\rangle = 34$ μm. Similar results were indicated in the deuterium runs but were not so certain since multiple scattering dominated much more.

The standard deviation of ρ^{-1} in each view is assigned an additional error σ_F. This is found to be somewhat larger than what is expected from setting errors (0.4×10^{-6} cm^{-1}). It is nearly the same in all 14 rolls, namely $(0.9 \pm 0.2) \times 10^{-6}$, $(0.7 \pm 0.2) \times 10^{-6}$, and $(0.8 \pm 0.2) \times 10^{-6}$ cm^{-1} in views 1, 2, and 3, respectively. The errors quoted are the standard deviations of the samples. Expressed as a standard deviation of the sagitta on the film plane over the entire track (12 cm) and after subtraction of setting error they are, in the three views, 2.0 ± 0.5, 1.3 ± 0.5, and 1.6 ± 0.4 μm, respectively. In the data taken with fixed distortion parameter (α_4) the corresponding values were 2.3, 2.5, and 2.6 μm. Thus we find that the refitting of α_4 for each frame and view improved the data. That this is so, means that the measurements of the fiducial marks are sufficiently precise to allow this to be done. We recall that in the deuterium runs, where a fixed α_4-term was applied, view 2 showed a rather large film error. Part of this improvement could, however, be due to the higher optical quality of the port windows in front of each camera. The main reason to re-fit the α_4 term would be to remove systematic film curvatures rather than to gain the small precision in the random error.

The setting error was studied, as in the deuterium run (see Fig. 9), with the help of the two deep minima in the curves of the standard deviation of the residuals as a function of x. A large number of such curves were studied (126 in all). The results for the setting error (ε) are shown in Fig. 16. Again it is found that the "setting error" increases with the flash time. If this is attributed to the fluctuating velocity of thermal eddies, one should expect the "setting error" ε to be given by

Table 10

Curvature random errors

Roll	Standard deviation [a] of $\rho^{-1} \times 10^6$ cm^{-1}			Correlation coeff. [b] for view pairs			Covariance [c] of curvatures $\times 10^{12}$ cm^{-2}			
	View 1	View 2	View 3	(1,2)	(2,3)	(3,1)	View(1,2)	View(2,3)	View(3,1)	Average
E0.8	1.99	2.04	1.97	0.75	0.84	0.79	3.04	3.38	3.10	3.17
E1.2	2.67	2.38	2.38	0.80	0.93	0.79	5.08	5.27	5.02	5.12
E1.6	2.12	2.12	2.12	0.84	0.86	0.82	3.78	3.87	3.69	3.78
E2.0	2.15	2.25	2.17	0.84	0.87	0.81	4.06	4.25	3.78	4.03
S0.8	1.68	1.65	1.57	0.83	0.86	0.79	2.30	2.23	2.08	2.20
S1.2	2.12	1.86	1.86	0.81	0.89	0.76	3.19	3.08	3.00	3.09
S1.6	2.49	2.25	2.33	0.89	0.92	0.84	4.99	4.82	4.87	4.89
S2.0	2.28	2.20	2.33	0.88	0.92	0.86	4.41	4.72	4.57	4.57
L0.8	1.83	1.81	1.97	0.87	0.87	0.83	2.88	3.10	2.99	2.99
L1.2	1.99	1.87	1.94	0.85	0.88	0.75	3.16	3.19	2.90	3.08
L1.6	2.04	2.02	2.02	0.90	0.90	0.87	3.71	3.67	3.59	3.66
L2.0	2.59	2.46	2.49	0.94	0.95	0.93	5.99	5.82	6.00	5.94
S1.2*	1.78	1.65	1.83	0.82	0.87	0.77	2.41	2.63	2.51	2.52
S1.2**	2.07	1.89	2.02	0.82	0.86	0.79	3.21	3.28	3.30	3.26

a) Error: $\pm 0.08 \times 10^{-6}$ cm^{-1}

b) Error: ± 0.02

c) Error: $\pm 0.2 \times 10^{-12}$ cm^{-2}

*) Loop 2 cooler than normal

**) Loop 2 still cooler

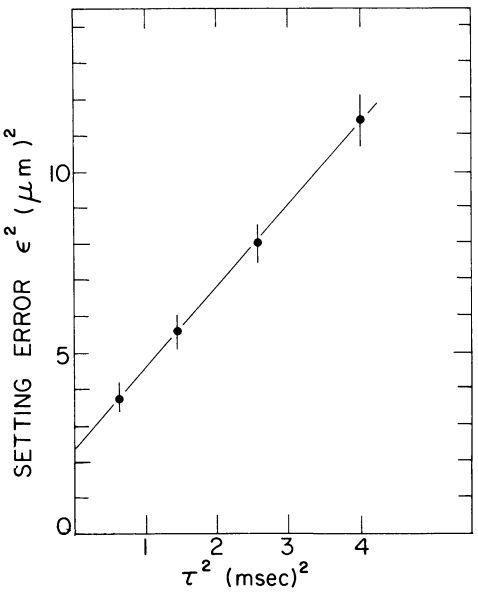

Fig. 16

The setting error (ε) on film in dependence of flash time delay (H_2-run). Each point is the average of 18 independent observations in each view. The line corresponds to

$$\varepsilon = \sqrt{1.5^2 + 1.5^2\tau^2}\ \mu m$$

with flash time delay (τ) in msec.

$$\varepsilon^2 = \varepsilon_0^2 + (\bar{\bar{\nu}} \cdot \tau)^2 ,$$

where $\bar{\bar{\nu}}$ is a r.m.s. velocity component. We find

$$\varepsilon_0 = 1.5 \text{ μm}$$
$$\bar{\bar{\nu}} = 1.5 \text{ μm/msec (on film)} .$$

Magnifying to chamber space gives 2.0 cm/sec as the r.m.s. velocity of HPD master points. This would correspond to about 4-5 cm/sec for the eddies themselves.

This is the order of magnitude expected [see Thomas[7] and Reinhard[8]]. The value $\varepsilon_0 = 1.5$ μm represents the HPD setting error and any contribution from scattering of the light-rays in the liquid.

The curves of standard deviations of residuals versus x show, beside multiple scattering contributions, a component attributed to liquid bulk motion fluctuations of about ±30 μm. This confirms the result obtained from the random distribution of curvatures.

5. CONCLUSIONS

i) Liquid convections of two types have been studied. One type is a large-scale liquid motion which acts to curve the tracks. The other is believed to be small-scale (eddies), which contributes to the setting error.

ii) Early timing conditions are best for high precision, i.e. beam arrival at about 2 msec before pressure minimum and a flash time delay $\lesssim$ 1.6 msec.

iii) The precision in the chamber is about ±30 μm on sagittas of 1.5 m long tracks. If the small-scale effect of eddies is added, one gets about ±40 μm as the precision on master points (averaging bubbles on about 2 cm).

iv) Systematic deviations of 30 μm can occur locally even under early timing conditions.

v) Errors due to variable film curvature can be reduced if for each frame a parabolic distortion term is fitted to the fiducial mark measurements, provided a sufficient number of fiducials are measured with HPD accuracy. For the film used here, this removed a sagitta jitter of about 2 μm r.m.s. on the film.

Acknowledgements

Two of the authors (G.E. and L.V.) would like to express their thanks to the Department Director Ch. Peyrou for making this study possible during their stay at CERN. Decisive contributions in the early planning stage were made by L. Montanet, H. Blumenfeld and M. Dykes, and K. Knudson took care of the data-processing. Many people helped in various phases -- the chamber crew, the scanning staff, the HPD experts and computer experts -- and their assistance is gratefully acknowledged.

* * *

REFERENCES

1) R. Budde, A. Burger, H. Filthuth, Y. Goldschmidt-Clermont, H.M. Mayer, D.R.O. Morrison, Ch. Peyrou and J. Trembley, Nuovo Cimento 14, 778 (1959).

2) H. Blumenfeld, A. Martinez, L. Montanet and J. Rubio, A study of the accuracy obtained with the 2 metre liquid hydrogen chamber in measurements of the K^0 and Λ^0 masses, Report CERN/D.PH. II/Phys 70-31 (1970).

3) Proc. Int. Conf. on Bubble Chamber Technology, Argonne 1970 (ed. M. Derrick) (ANL, Batavia, Ill., 1971); (see for example, paper by P. Slattery and references given therein).

4) W. Blair, private communication.
P. Berge, CERN D.PH II/LSD 71-5b/, 18 May 1971.

5) G. Ekspong, Multiple scattering residuals on tracks, CERN/D.PH II/Phys 71-40/(1971).

6) K. Gluckstern, Nuclear Instrum. Methods 56, 145 (1967).

7) D.B. Thomas, Turbulent convection in hydrogen bubble chambers and associated optical distortions, Rutherford Laboratory report, 1966.

8) H.P. Reinhard, Report CERN/TC/BEBC 66-62 (1966).

APPENDIX

THE MULTIPLE SCATTERING CONSTANT

We define K as the proportionality factor relating the variance of small space-angle scattering to track length L according to

$$\text{var } \Theta = KL \frac{1}{(p\beta c)^2} \quad .$$

The projection factor (= 1/2) for scattering angles in one plane will be introduced explicitly. Following Gluckstern[6] we get in the small-angle approximation

$$\frac{1}{L} \text{ var } \Theta = \sum_i N_i \, 2\pi \int_{\Theta_{min}}^{\Theta_{max}^{(i)}} \Theta^3 \, \sigma(\Theta) \, d\Theta = \sum_{i=1}^{2} N_i \frac{8\pi e^4}{(p\beta c)^2} \left(\ln \frac{\Theta_{max}}{\Theta_{min}} \right)_i \quad ,$$

where in deuterium the summation is over the scattering centres (i = 1 nuclei, i = 2 electrons). With the expanded density of deuterium at 31.2°K given by $\rho = 0.139$ g cm^{-3}, we have

$$N_1 = N_2 = 41.6 \times 10^{21} \text{ cm}^{-3} \quad .$$

The value of Θ_{min} is given by the ground state of atomic hydrogen as

$$\Theta_{min} = \frac{4.2 \times 10^{-3}}{p} \qquad \text{(with p in MeV/c)} \quad .$$

The remaining problem in computing the scattering constant concerns the value of Θ_{max}. Gluckstern considers three possibilities given by a) the kinematic limit, b) visible nuclear recoil track, and c) minimum of detectable angle. As we carefully eliminated tracks with single scatterings, we find that our average limit for detectable scatterings lies at 2.2 mrad for nuclear scattering and 1.8 mrad for scattering on electrons. These values are smaller than the other two limits (visible recoil gives about 5.6 mrad and the kinematic limit in the case of electrons is $M_e/M_\pi = 3.7$ mrad). Thus the sum is

$$\sum \ln \frac{\Theta_{max}}{\Theta_{min}} = \ln \frac{2.2p}{4.2} + \ln \frac{1.8p}{4.2} \quad .$$

With p = 16,000 MeV/c we finally get

$$K = 0.357 \text{ MeV}^2 \text{ cm}^{-1} \quad ,$$

which we consider good to a 10% uncertainty. It is noted that for L = 1.6 m the limits on Θ_{max} correspond to angles in the region of 4 standard deviations, thus effectively excluding the tails outside the central Gaussian distribution.

In fits to a parabola the variance in the curvature parameter c ($y = a + bx + cx^2$) is given by

$$\text{var } c = \frac{\frac{1}{2}K}{(p\beta c)^2} \cdot \frac{1}{3L} \cdot \frac{15}{14} \quad ,$$

valid for a very large number of points on a track (for comparison the factor 15/14 is to be replaced by 1.0 in the case of only three points). From this and the relation $c = 1/2\rho$ we compute the multiple scattering variance as var $(\rho^{-1})_{m.sc.} = 6.11 \times 10^{-12}$ cm^{-2} ($\pm 0.6 \times 10^{-12}$) and $\sigma(1/\rho) \equiv \sqrt{\text{var } 1/\rho} = 2.47 \times 10^{-6}$ cm^{-1} ($\pm 0.12 \times 10^{-6}$) on 16 GeV/c tracks of length 1.63 m. The quoted errors refer to a possible ±10% uncertainty in the scattering constant.

Note

The multiple scattering in the xz-plane is seen to some extent by the various cameras. The dominating component is the scattering in the xy-plane with a contribution from the xz-plane of about 0.2% to 2.5% in the variances. In the covariances a negative correlation should act to reduce the value for the view-pair (1,3) by about 1.5% and less in other view-pairs. As these corrections are small they have not been applied.